University of Kerbala
College of Science
Department of Chemistry

Preparation and Characterization of $CoFe_2O_4$/ Activated carbon/ Polyaniline as a Ternary Composited their application in water treatment

A Thesis

Submitted to the Council of the College of Science/ University of Kerbala

In a Partial Fulfillment of the Requirements for the Degree of Master of Science in Chemistry

By

Mohammed Fadhil Hateef

B.Sc. Chemistry (2016) / University of Kerbala

Supervised by

Assist Prof. Dr. Hasan Fasil Alesary

Prof. Dr. Luma Majeed Ahmed

2025 AD

1446 AH

بسم الله الرحمن الرحيم

﴿يَرْفَعِ اللَّهُ الَّذِينَ آمَنُوا مِنكُمْ وَالَّذِينَ أُوتُوا الْعِلْمَ دَرَجَاتٍ﴾

صدق الله العلي العظيم

سورة المجادلة
الآية (11)

Supervisor Certification

We certify that this thesis, entitled " Preparation and Characterization of $CoFe_2O_4$/ Activated carbon/ Polyaniline as a Ternary Composited their application in water treatment " has been prepared under my supervision, by **"Mohammed Fadhil Hateef"** at the department of Chemistry, College of Science, University of Kerbala in a partial fulfillment of the requirements for the degree of Master of Science in Chemistry

Signature:

Name: Dr. Hasan Fasil Alesary
Title: Assist Professor
Address: University of Kerbala, College of Applied Medical sciences
Date: / /2025

Signature:

Name: Dr. Luma Majeed Ahmed
Title: Professor
Address: Al-Zahraa University for Women, Karbala, Iraq.

Date: / /2025

In view of the available recommendations, I forward this thesis for debate by the examining committee.

Signature:
Name: Dr. Sajad Hassan Guzar
Title: Professor
Head of the Chemistry Department, college of science/ University of Kerbala
Date: / /2025

Examination Committee Certification

We certify that we have read this thesis entitled "" Preparation and Characterization of $CoFe_2O_4$/ Activated carbon/ Polyaniline as a Ternary Composited their application in water treatment " as the examining committee, examined the student " Mohammed Fadhil Hateef " on its contents, and that in our opinion, it is adequate for the partial fulfillment of the requirements for the Degree of Master in Science of chemistry.

Signature:

Name: Dr. Ahmed Hadi Al-Yasari
Title: Professor
Address: University of Kerbala, College of , College of Applied Medical sciences
Date: / /2025
(Chairman)

Signature:

Name: Dr. Ihsan Mahdi Shaheed
Title: Assist Professor
Address: University of Kerbala, College of Science, Department of Chemistry
Date: / /2025
(member)

Signature:

Name: Dr. Ahmed Fawzi Halbus
Title: Assist Professor
Address: University of Babylon, College of Science, Department of Chemistry
Date: / /2025
(member)

Signature:

Name: Dr. Hasan Fasil Alesary
Title: Assist Professor
Address: University of Kerbala, College of , College of Applied Medical sciences
Date: / /2025
(member& supervisor)

Signature:

Name: Dr. Luma Majeed Ahmed
Title: Professor
Address: Al-Zahraa University for Women, Karbala, Iraq.
Date: / /2025
(member& supervisor)

Approved by the council of the College of science

Signature:

Name: Dr. Hassan Jameel Jawad
Title: Professor
Address: Dean of college of science/ University of Kerbala
Date: / / 2025

Dedication

To my imam and master, the owner of the time (may God hasten his honorable return), the light of hearts and the inspirer of souls, I ask God to grant me His intercession and satisfaction and to make this work of mine an asset for the sake of the truth that humanity awaits. To my dear parents, the source of love and giving and the foundation of success in my life, to those who gave their lives for me, and they were the light that illuminated my path and the hand that supported me at every step. And to my dear wife, my life partner and supporter of my career, who has always supported me with her patience and love and brightened my days with her sacrifices and wishes for my success. I dedicate this humble work to you, hoping to God that it will meet your good expectations and be an asset for the hereafter.

Acknowledgments

Praise be to Allah, Lord of the Worlds. May God's blessings be upon Mohammed and his pure personal family, and thank God for his numerous graces and gifts.

I am grateful to my supervisors, Assist. Prof. Dr. Hasaan Fasil and Prof. Dr. Luma Majeed Ahmed, for their ongoing support and insightful ideas during this project.

I also like to thank all faculty members from the Department of Chemistry in the College of Science at the University of Kerbala. Finally, I want to thank my family and friends for their ongoing support throughout this journey. They were a source of inspiration for me throughout the process.

Abstract

This work involves three parts, the first of which utilizes a new deposition process to synthesize cobalt ferrites ($CoFe_2O_4$) nanoparticles using cetramide (CT) as a positive surfactant. The $CoFe_2O_4$ nanoparticles were synthesized as an inverse spinel. The PANI/$CoFe_2O_4$/Ac nanocomposite was created by a chemical oxidation polymerization process with hydrochloric acid and Ammonium Persulfate (APS) as activators and oxidants.

Through the second part, spinel $CoFe_2O_4$ nanoparticles and their composites were identified by several techniques. Infrared spectroscopy showed characteristic peaks between 400 and 600cm^{-1}, indicating the locations of tetrahedral Fe-O and octahedral Co-O isoforms in the $CoFe_2O_4$ nanoparticles. X-ray diffraction showed that the prepared samples of $CoFe_2O_4$ and its ternary composite have nanoscale size ranged from 31.83 nm for $CoFe_2O_4$ to 36 nm for the ternary composite. The SEM image showed an idea of the surface morphology of the prepared compounds, the shape of the $CoFe_2O_4$ spinel was found to be texture-like, but for composite was found to be layered, the particle sizes measured of the spinel were found to be between 33.03 to 41.35 nm, and for the composite equal to 29.34 to 49.90 nm, thus, all samples studied are considered to be nanocrystals. The EDX spectra showed that the Co, Fe, O, and C elements of the catalyst were present and pure with no impurities. The BET surface areas and pore size distribution were measured for both synthesis samples and demonstrated the hysteresis loops correspond to the adsorption isotherms of type IV, and the hysteresis loop in the relative pressure range (P/P0) of 0.3~1.0, which belongs to type H3 with nanopores. The specific surface area of ternary composite is of more value for cobalt ferrite and equal to 54.118 $m^2\ g^{-1}$ and 8.9064 $m^2\ g^{-1}$, respectively.

In the third part, $CoFe_2O_4$ /AC/ PANI were used as adsorbent for the removal of direct orange dye from aqueous solutions. Initially, the adsorption experiment was carried out for all the prepared surfaces towards the dye and the highest percentage of dye removal was found on the superimposed surface where the removal rate reached 95%.

The removal efficiency of direct orange dye was found at 45 minutes as optimum equilibrium time, surface mass at 0.3 g, and pH 6, temperature 25 c and 5 mg\L concentration After that, the factors affecting the adsorption process (time, concentration, weight, pH, temperature) were studied for the surface of cobalt ferrite and ternary composite, and the ternary composite gave a higher removal efficiency compared to cobalt ferrite. In reusability, it was found that after four cycles, the dye removal efficiency of the composite decreases from 95.24% to 70.11%, while the dye removal efficiency of cobalt ferrite decreases from 82.34% to 28.35%. These results indicate that the composite shows higher reusability compared to cobalt ferrite.

On the other hand, the thermodynamics functions were detected and was found that removal reaction of dye by $CoFe_2O_4$ is exothermic with physical adsorption (less than 40 kJ/mol). this result is in agreement with the result via applied Freundlich equation, while the same reaction using composite was demonstrated a chemical adsorption (greater than 80 kJ/mol) with endothermic reaction. The PFO model is obeyed the adsorption of direct orange 39 dye onto the $CoFe_2O_4$ /AC/ PANI and CoFe2O4 nanocomposite adsorbent, because correlation coefficient R^2 for PFO > correlation coefficient R^2 for PSO,

List of Tables

List of Figures

List of abbreviations and Symbols

Abbreviation	The Meaning
(APS)	Ammonium Persulfate
ΔG	Change in free energy.
ΔH	Heat of Adsorption
ΔS	The change in entropy
ΔG	The change in free energy
ΔH	The heat of adsorption
ΔS	The change in entropy
A	Adsorption
AATCC	American Association of Textile Chemists and Colorists
AC	Active carbon
BET	Brunauer–Emmett–Teller
CCP	Cubic Close-Packed
C_e	The equilibrium concentration
CTAB	cetyltrimethylammonium bromide
D	The crystallite size of the particle
E%	The percentage of dye removal
JCPDS	**Joint Committee on Powder Diffraction Standards،**
k	The Scherer Constant
k_e	The equilibrium constant
k_f	Empirical Freundlich constant.
k_L	The Langmuir isotherm constant.
Oh	Octa hederal.
PANI	Polyaniline
Q_e	The quantity of solute adsorbed
R	The Gas Constant
SDC	Society of Dyers and Colourists
SDS	Sodium dodecyl sulfate
SEM	Scanning electron microscopy.
Th	Tetra Hederal
XRD	X-ray diffraction spectroscopy
β	Full-Width A half-maximum
θ	Bragg angle
λ_{Cu}	Wavelength of the Cu lamp in an X-ray apparatus

Chapter One
Introduction

Chapter One Introduction

1.1. General Introduction

The level of water pollution has been increasing over the decades mainly because of the growth of industrialization. This phenomenon is dangerous to human health, animal life, natural resources and the environment at large (1). Comparing different types of water pollutants, it is worth mentioning that aromatic organic materials like dyes and pigments are applied in textile industry, plastics, paper, leather, food stuffs, cosmetics and hair dye industry. In the world, an estimated 700000 metric tons of dyes are produced every year (2). The toxicity and non-biodegradability of the unreacted dyes released into water bodies make them a menace to the environment. Azo dyes contain one or more of –N=N– bond, preprepared diazo compounds or diazotized amines, which forms through coupling with amines and phenols. These dyes settle in water bodies with great affinities for water and water soluble and lower the dissolved oxygen content, thus posing great impacts on the ecology of water bodies (3), for example: Direct Orange Dye, which belongs to benzidine azo compounds is used in dyeing of paper textiles and yarns and in laboratories for pH indicators. However, it is highly toxic even in concentrations of less than one part per million, which have carcinogenic, mutagenic and dermatitis-like effects. When metabolized, benzidine that is set free from direct orange dye causes severe health complications such as respiratory disorders, blood coagulation dilemma and somnolence (4). Direct orange dye is found to react with water and form various compounds in aqueous solution based on their pH. Ther fore, a strong need for methods to the removal from dye. Coagulation- precipitation, Biochemical treatment, activated sludge, ozonation, reverse osmosis, filtration, photocatalytic degradation, adsorption(5). Although such approaches have advantages for high-quality work, its drawbacks include high costs, low work rates, and energy demands. In adopting the available

separation techniques, adsorption turns out to be among the most effective and economical solutions especially when applied alongside the right adsorbents [6]. Indeed, polyaniline (PANI), the adsorbent used here, possesses two active groups of nitrogen, namely amine group (-N<), and imine group (-N=), both of which have free ion pairs of electrons in their structures that can readily interact with direct orange dye. In general, the aim interactions between polyaniline as based adsorbent and dye as an adsorbate included π–π interaction, hydrogen bonding, and electrostatic attraction. Methyl orange anionic pollutant can form a complex with emeraldine salt of PANI; which is cationic in nature in acidic aqueous medium due to electrostatic attraction. The Following are Factors that influence adsorption process: the functional groups present on the adsorbent and the functional groups present on the adsorbate. Adsorbent shape and porosity. Diffusion constraints between the adsorbent and the adsorbate since the absorption mainly takes place on the surface (6)(7).It was also found that the PANI composites with carbonaceous compounds or metal oxides present higher dye removal efficiency than cobalt ferrite. These composites possess high mechanical strength large surface area, outstanding thermal stability, high electrical conductivity, increased porosity (8).

1.2. **Source of Water Pollutants.**

Water is polluted by several important sources, which can be identified as follows: wastewater sources figure (1) such as, domestic and industrial waste products, animal waste, dead organic material, chemicals such as soaps and industrial detergents and some forms of useful bacteria and microbes that are harmful…etc. Sources of oil and its derivatives: water contamination by oil involves the release of oil materials into bodies of water, incidence, mistakes in several types of searches, drilling, and

transport processe, Industrial sources. These include most wastes generated from industrial processes: chemical; mining; processing; manufacturing; food industries and other industries. Agricultural sources: these are Chemical fertilizers' pesticide and agricultural fertilizer (Phosphorus and nitrate compounds). Natural sources: expressed in the form of rainfall, animal droppings Planted or cultivated produce, waste products, deposits and earth-like substances(9).

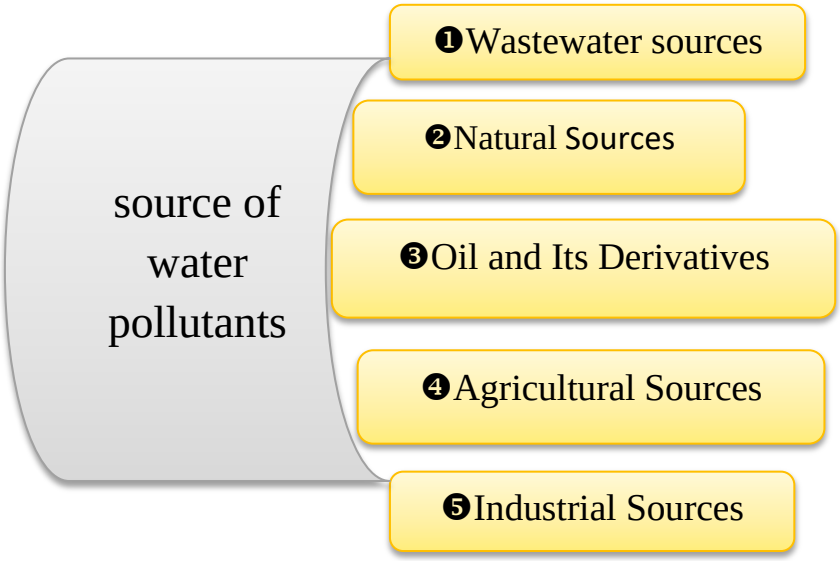

Figure (1.1). Source of water pollutants.

1.3. Dyes.

Dyes are common in many industries such as textile, fashion, paper, plastics and polymers, food industries, printing and visuals arts, cosmetics and pharmaceuticals. Generally, most dyes are organic compounds containing different functional groups and complex aromatic systems[12]. Nevertheless, some colors that find their way into receiving streams through industrial effluents are potential polluters of water. The dyes and

most products of degradation of dyes are mutagenic, and carcinogenic, allergenic and toxic most of which when released in the environment causes the environment fitness both humans and aquatic life resulting to chronic and acute diseases. However, some dyes that are let into receiving streams in industrial effluents could pollute the water. Because of the given conditions in which the colors in water effluents are not safe Most dyes and their breakdown products are extremely toxic to humans and aquatic life. They are also carcinogenic, allergic, and mutagenic. This may cause both short-term and long-term disorders , [13] [14] Because dyes are generally characterized by their relative molecular weight and modified stability, the methods of their removal from wastewater include chemical, biologic, and physical procedures, such as photolysis, adsorption, precipitation of chemical compounds, nonchemical destruction, and electrochemical precipitation(10)(11). (12).Direct Orange 39 is a synthetic azo dye which is used as a cellulose dye to dye cotton among others through Teachable class of dyes. Mainly employed in application of dyes or printing of woven and knitted materials made from Cellulosic fibers including cotton. Can also be utilized in paper coloring as well as some industrial uses where its bright orange color characteristic of the chemical is desirable. It forms an orange color which is very bright. Good affinity for cellulose fibers since it is a direct dye and thus does not require a mordant to attach to the fibers. As for Fastness, it has a moderate light fastness and wash fastness with slight stanching but this may differ according to the type of utilization and end post treatment impact on nature and human health. As with many other azo dyes, Direct Orange 39 may produce aromatic amines in some situations and, therefore, poses environmental and health risks. Interceptors emanating from industries utilizing this dye should be well managed to reduce harm

to the environment.(13). The common properties and structure of this dye is demonstrated in figure (1.3) and table (1.2).

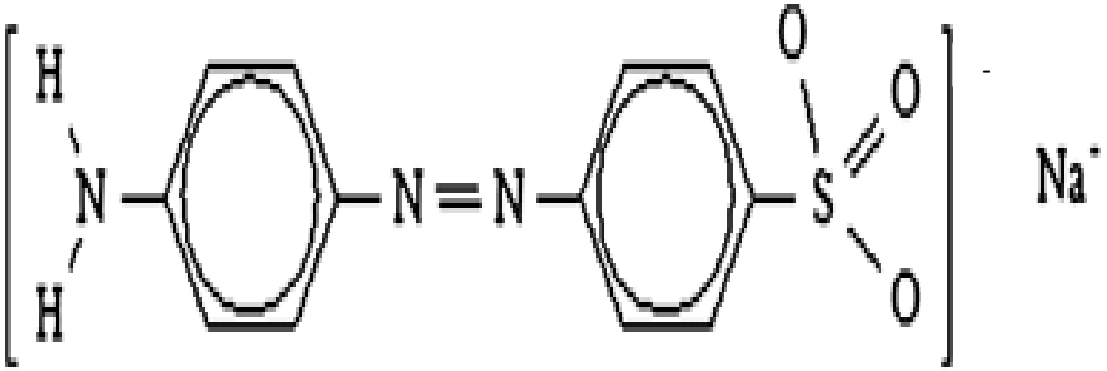

Figure (1.2)Chemical structure of Direct Orange 39 dye(14)

Table (1.1) Some of the features which can be associated with the Direct orange 39 dye(15)

The variables	**Information**
Molecular Formula	$C_{12}H_{10}N_3NaO_3S$
Molecular Weight	299.281 g mol^{-1}
Common Synonyms	Solar Yellow 3R and Orange 2GL
Dye Class	Azo, Direct Dyes
λ_{max}	415 nm

1.4. Classification of dyes

The list of dyes was initially prepared by the SDC, and the society published it jointly with the AATCC (Color Catalog Volume was published for the first time in 1924, which is considered to be the official source of dyes(16). Dyes are primarily classified based on their chemical

structure or their method of application [22. From this perspective, each dye is associated with a specific classification system. The numerical classification (Colour Index – Constitution Number, CI-CN) reflects the chemical characteristics of the dye, while the nominal classification (Colour Index Name, CI Name) corresponds to its application method [23].

1.4.1. Chemical classification:

The classification of colors based on their structures as chemicals is mainly based on the chemical nature of the chromophore group the study of the classification is relevant to the manufacturer of coloring materials and dyes. There are many categories, the most important of which are Azo dyes that contain one or more azo groups (-N=N-) and anthraquinone dyes Which is a chemical defined by the presence of two aromatic rings joined by two carbonyl groups(O=C) in each molecule Pigment has a systematic name within these chemical categories (17). The dyes can also be classified according to the source of chemicals used in synthesizing the said dye in xanthene's, heterocyclics, nitro, stilbene, phthalocyanine, indigoid, polymethine, and anthraquinone.

1.4.2. Applied classification:

This type of classification is based on the presence of auxochrome groups in dye molecules. However, for practical purposes in the textile industry, classification based on the application method is considered more appropriate, as it directly relates to how dyes are used in different materials and processes.

There are various techniques for applying dyes, but a common requirement across all methods is that the dye must be water-soluble at

some stage of the dyeing process. Some dyes are naturally highly soluble in water, while others require chemical modification to achieve solubility.

Based on the application methods, dyes are classified into several categories, each tailored for specific dyeing techniques and fiber types [25].

1.5. Spinel Semiconductor

Regarding the structure of spinel, it is a mixed oxide which can be described in a general form AB_2O_4 where A and B may be respective cations that contain some of the following elements and are used in some aspects such as catalytic ones. Indeed, it is a substance that is also heat stable and chemically conservative as well. In the oxide, there are one divalent and two trivalent Fe cations which mean the average of cation, charge is 2+ such as magnetite Fe_3O_4 which chemically consists of iron (III) oxide with a spinel structure which is perfectly stoichiometric. Chemically conservative as well. In oxides there are one divalent and two trivalent Fe cations which gives an average of cation charge of 2^+, such as magnetite Fe_3O_4, which has been found to be chemically composed of iron III oxide with a spinel-like structure which is considered to be perfectly stoichiometric. That is why most of the catalytic properties of spinels are reported to be dependent on the presence of cations with diverse charges which incite internal redox reactions and the reduction-reoxidation cycles of the catalyst. In the spinel, oxygen anions are nearly in CCP array, and the cations are accommodated in the available space. Concerning the A sites which form a very little part of the interstices, out of the counter's total tetrahedral interstitial sites only eight can accommodate Mn (18).

1.5.1. Classification of spinel semiconductors.

Spinel semiconductors are classified into two types based on their charge transport mechanisms:

1. **N-Type Spinel Semiconductors** Charge Transport Mechanism: the process involves hopping electron conduction (e^-) between iron ion sites in the octahedral structure. Reversible electron conductivity: The Fe^{3+} and Fe^{2+} redox couple, represented by the reaction $Fe^{3+} + e^- \leftrightarrow Fe^{2+}$, demonstrates that the concentration of Fe^{2+} increases the reversibility. Mechanism for Conductivity Enhancement: Oxygen chemisorption on n-type spinel ferrite changes Fe^{3+} to Fe^{2+}. Oxygen oxidation and reduction of dyes release e^-, increase Fe^{3+}/Fe^{2+} couples, and improve electrical conductivity. The oxidation-reduction reaction at n-type spinel ferrite surfaces is reversible. Examples are $MgFe_2O_4$, $CdFe_2O_4$, $ZnFe_2O_4$, and $CoFe_2O_4$.

2. **P-Type Spinel Semiconductors** are inverse spinel ferrites with transition metal ions (M^{2+}) at the octahedral and Fe^{3+} at the tetrahedral sites. Charge Transportation Mechanism: Hole (h^+) hopping conductivity of Ni^{2+} and Ni^{3+} at octahedral sites: $Ni^{2+} + h^+ \leftrightarrow Ni^{3+}$. During synthesis, oxygen ions absorb Ni^{2+} and convert it to Ni^{3+}, creating cation vacancies. Example: $NiFe_2O_4$ (19).

1.6. **Adsorption**

Adsorption is a longstanding and intricate chemical and physical process with significant potential for producing effluents of acceptable quality. This phenomenon can be called extraction of liquid- solid because of

depending on the bending forces between liquid and solid surface (20), Thereby the compounds adhere to the outer layer. with formation of an excess concentration on the outer layer. As pointed above, adsorption is a spontaneous process entails of reduction of the system free energy and entropy (21). This is the case causes the increasing in ordering of molecules at the surface to be more ordered than the molecules in solutions. The force that binds the adsorbate and the adsorption surface is due to many more highly differing forces such as dispersion force and dipole interaction.

1.7. Types of Adsorptions

Depending on the type of affected forces on adsorption, the adsorption can take one of two forms: chemical adsorption (chemisorption), or physical adsorption (physisorption) (19), as listed in Table (1-1).

Table.1.2.The different between Physisorption and Chemisorption (20)

Physisorption	Chemisorption
Dictated by van der Waals forces.	Chemical bonds are the basis of forces.
Heat of adsorption is Less than 40 kJ mol^{-1}.	Heat of adsorption surpasses 80 kJ mol^{-1}.
There is no transfer or exchange of electrons between the adsorbed species and the adsorbent surface. When the condition is not met, the event takes place to release activation energy.	The outermost layer of the adsorbent and the adsorbate undergo electron sharing or exchange. Vitality for It could be necessary to activate.
The process is standard.	The process stands out due to its uniqueness.

Long-range operation of the forces may result in multilayer adsorption	After adsorption, a monolayer is created, and inclusion may follow.
Only at temperatures lower than the boiling point of the adsorbate can adsorption be detected.	Adsorption may take place at elevated temperatures
It is possible to reverse the procedure. The adsorbing layer can be removed by heating the region to a low temperature or by emptying it.	It is possible to reverse the procedure. The adsorbing layer can be removed by heating the region to a low temperature or by emptying it.

1.8. Mechanisms of Adsorption in Solution

The adsorption process from a solution onto a solid adsorbent surface, is unlike the single-substance adsorption (gases, vapors, or pure liquids), because of it involves multi-component solutions generating a thicker layer on the surface that is demonstrated in figure (1.2) The key steps include: (21).

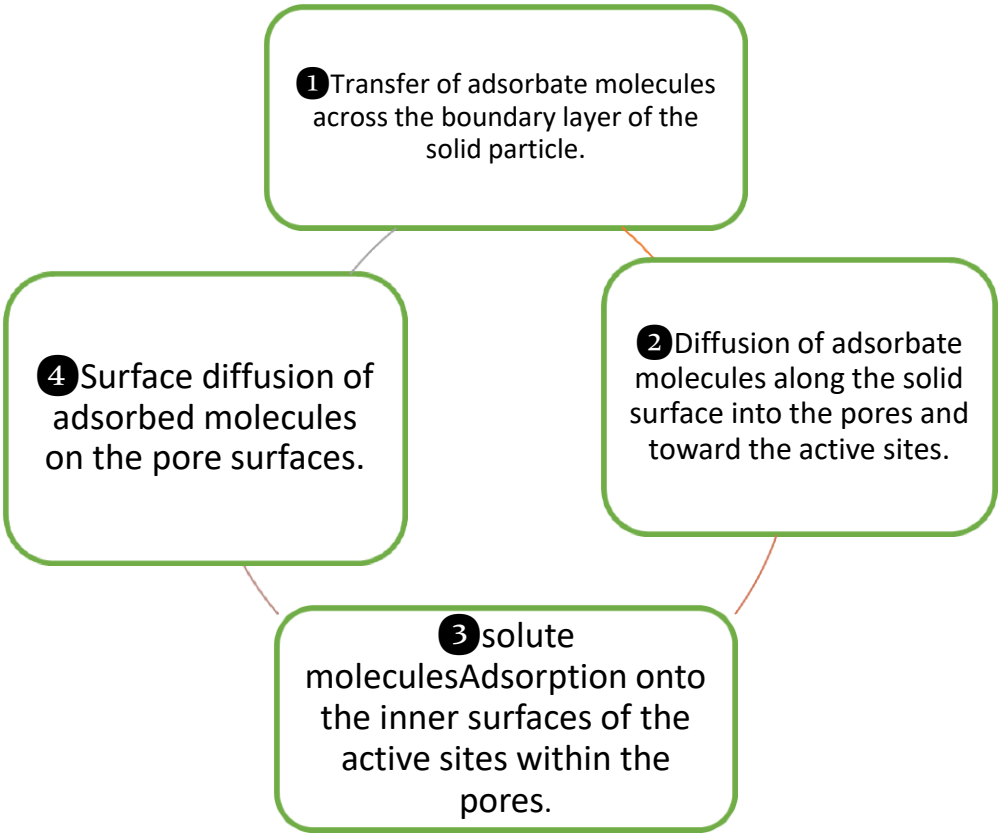

Figure (1.3). The key steps adsorption mechanisms in Solution

1.9. Factors Affecting the Adsorption Process

The adsorption process is influenced by the following variables:

1. **Concentration of adsorbate**

   A constant temperature environment produces an increased amount of material that adheres to a specific adsorbent mass with increasing solute concentration (22).

2. **Temperature**

   The type of adsorption and the characteristics of the adsorbent and adsorbate determine how temperature affects the extent of adsorption. Lech atelier's Principle states that a drop in system temperature would cause a reduction in temperature that increases the extent of adsorption

like chemisorption, and that increases adsorption like physical adsorption (23)

3. **Effect of pH**

   Because pH affects the chemical states of the adsorbent, adsorbate, and solvent, adjusting the pH of the solution has a significant impact on the amount of adsorption that can occur from the solution. Because of the disagreement between OH^- and H^+, This effect is observed with ions and their overlap with the solvent, adsorbate, or adsorbent surface (24).

4. **Nature of the adsorbate**

   The adsorbate's chemical and physical properties determine the extent to which adsorption occurs. A molecule's ability to adhere to a surface is determined by its size, stereochemistry, polarity, and the presence of distinct persistent groups (25).

5. **Adsorbent surface area**

   The particle size and surface area of a given mass of adsorbent are inversely related. That is, the smaller and more porous or finely divided the material is, the greater its specific surface area. A higher surface area increases the number of available active sites for adsorption, thereby enhancing the adsorptive capacity of the material. Consequently, as the number of surface-active sites increases, the material becomes more effective at adsorbing target molecules [21].

1.10. Classification of Adsorption Isotherms

The adsorption process is generally analyzed using graphs called adsorption isotherm. Adsorption is the quantity of adsorbate on the adsorbent for a given pressure/ concentration of the adsorbate at a constant temperature. The quantity adsorbed is specificed by mass of the

adsorbent so that comparisons between different materials can be made. Hence, it can predict that after saturation pressure, adsorption does not occur anymore. that is, there are limited number of vacant places on the adsorbent. When pressure is high, all the sites are filled and further raised pressure does not make any variation in the overall adsorption. At high pressure, adsorption has no effect with pressure(26).

Thus, depending on the Chara constructive physical and chemical properties of the curve characteristic at low concentrations of the adsorbate solution, the classification of isotherms is given in figure (1-3). Giles and colleagues established the following four main types of adsorption isotherms(27) (28).

❶ L-Type (Langmuir Type) Characteristics

This isotherm implies that a one-layer deposit is formed on a uniform surface only. The adsorbent surface is characterized by a finite number of identical and indistinctive binding sites. Adsorption is carried out without much hindrance from the solvent phase physisorption competes weakly with chemisorption.

Mechanism: the main direction of the six adsorbate molecules is parallel to the surface formed by the six base atoms.

Applications: characterized by reversible binding of gas molecules on solid surfaces.

❷ H-Type (High Affinity Type) Characteristics:

The expresses preferential adsorption is based on close interaction between adsorbent and adsorbate. This can be observed even in solutions of a very low concentration.

Mechanism:

The adsorption mechanism can involve various processes, including chemical interactions (such as covalent bonding or redox reactions), polymer-based adsorption (where functional groups in the polymer interact with the target molecules), or the formation of ionic micelles (aggregates formed by surfactants that trap contaminants through electrostatic or hydrophobic interactions).

Applications: often linked towards the reactions as, for instance, ionic or chemical bond.

❸ S-Type (Cooperative Adsorption)

The characteristics demonstrates an early phase, which flattens with increasing concentration of solute, and suggesting various strong inter molecular forces within the adsorbed layer.

Mechanism: these solvent molecules are adsorbed very effectively in the initial stage, and afterwards the adsorbate is favored by cooperative interactions.

Applications: observed in systems in which adsorbate molecules stack up in one or several layers.

❹ C-Type (Constant Partition Type, Partition Constant Type, Partition having Fixed Type)

The characteristics are exhibiting linearity characteristics when the amount adsorbed is plotted against the concentration of the species being adsorbed. It shows an equilibrium between adsorbate and the solution phase as well as with the adsorbent material.

Mechanism: the solute particles take a shorter time to penetrate the adsorbent than the solvent particles.

Applications: the adsorption process depends on the strength of the interaction, which is similar to the forces between atoms including the van der Waals forces.

1.11. Thermodynamics of Adsorption

It is feasible to collect valuable information on the unpredictability, spontaneity, and binding strength of the adsorption process thanks to the thermodynamic treatment of adsorption. The thermodynamic functions that define adsorption from solution can be found by measuring adsorption isotherms at different temperatures in systems that exhibit reversible behavior. Adsorption studies at different temperatures (which result in the computation of thermodynamic data and their interpretation) clearly require the analysis of changes in solution density, changes in the solubility of substances with temperature (29).

One of the primary objectives of adsorption thermodynamics is the analysis of the thermal effects associated with adsorption. The heat of adsorption that forms when a single gas is absorbed by a solid is easier to comprehend than the heat change that occurs when a solution comes into contact with a solid. By measuring the concentrations required to produce a specific amount of adsorption at different temperatures, the heat of adsorption from solutions can be found. Compared to the same adsorbent from a gaseous phase, the heat of adsorption from solutions is frequently several times lower (30). Thus, the following equation could be used to calculate the heat of adsorption (ΔH):

$$\ln k = -\frac{\Delta H}{R} x \frac{1}{T} + C \qquad (1\text{-}1)$$

R: 8.314 is the universal gas constant in unite J/mol. K, k: The equilibrium constant for adsorption at various temperatures, T: Kelvin temperature.

Adsorption from solutions reaches equilibrium more slowly than adsorption from the gas phase. The equilibrium constant (keq) for the adsorption process at each temperature was calculated using the following formula. (31)

$$k_{eq} = \frac{q_e.m(g)}{C_e.V(L)} \quad (1\text{-}2)$$

where m is the adsorbent's weight (g), Qe is the amount adsorbed (mg/g), Ce is the adsorbate's equilibrium concentration (mg/L), and V is the adsorbate solution's volume (L). Equation can be used to compute the change in free energy (G).(32)

$$\Delta G^o = -RTlnk_d \quad (1\text{-}3)$$

The Gibbs energy ΔG^o was calculated using the universal gas constant (J/mol K) (R) and the absolute temperature (T). (33)(34)

$$k_d = \frac{C_{ads.}}{C_e} \quad (1\text{-}4)$$

$$\Delta G^o = -RTlnk_d \quad (1\text{-}5)$$

The enthalpy change ΔH^o and entropy change Therefore, the Vant Hoff equation was used to determine (35)

$$lnk_d = \frac{-\Delta H^o}{RT} + \left(\frac{\Delta S^o}{R}\right) \quad (1\text{-}6)$$

However, the activation energy was calculated using equation (1-6). (36)

$$E_a = \Delta H^o + RT \quad (1\text{-}7)$$

straight line with a slope of -ΔH^o/R and an intercept of ΔS°/R is produced when plotting ln kd vs. 1/T; the Gibbs equation can be used to determine.

1.12. Surfactants

These are called Surface Active Agents which facilitate the reduction of the interfacial tension or Surface Tension existing between two dissimilar phases which can be liquid/liquid, liquid/gaseous phase or liquid/solid phase. However, for photocatalysts with the core-shell structure, uniform spherical morphology, and multilayer hierarchical structure, the increased electronic transfer and optimal light absorption can improve the photocatalytic property(11).Surf- actants are amphiphilic molecules, both hydrophilic and lipophilic part have been established to form shape determining agents synthesizing photocatalysts. This is especially so since they define an average structure of catalysts by adsorption of surface-active species on different crystal planes in the nucleation center (37) Depending on the nature of the alkyl group and the charge of the hydrophilic portion, the surfactants can be divided into four categories with four subcategories(38) shown in table 1-3.

Table (1-3). The classification of surfactants, with common usages and examples (39)(40)(41)**.**

Types	Info.	Examples and used
Cationic surfactants	These species include additional alkyl groups or at least one hydrophobic hydrocarbon chain connecting to a positively charged nitrogen atom.	Trimethylammonium bromide (CTAB), quaternary ammonium compound (QAC), and cetrimide (CT) are used in fabric softeners, hair conditioners, and detergents.
Anionic surfactants	In this case, alkyl chains, alkylphenol ethers or alkyl benzene bonding to carboxyl, sulfate, sulfonate or phosphate constitutes the major part of hydrophobic segment of the molecule.	With respect to the former category, some of the examples are stearic acid (SA), sodium lauryl sulfate (SLS), and sodium dodecyl sulfate (SDS). Used in drug delivery systems, they form physical and chemical complex with the

		medicament thereby enhancing the effectiveness of the active ingredients.
Amphoteric surfactants	The latter is the pH that defines such species. These species demonstrate properties of having both positive and negative charges at the intermediate pH and can easily change the charge from cationic to anionic at low pH to high pH .	Amine oxide (AO) finds use as an antibacterial or deodorant in bars, a foam sterilant in rubber industry and polymerization catalyst in rubber industry, and an antistatic in the textile industry.
Nonionic surfactants	The long-chain linear alcohols, fatty acids and alkylated phenol derivatives with long hydrocarbon chain are the non-ionic surfactants which are hydrophobic in nature, whereas the ethylene oxide chain may vary in lengths and is hydrophilic in nature.	HMTA and n <3 FAEs serve as foam stabilization agents, wetting agents, and emulsifiers while n≥3 AE are employed as simple emulsifiers.

1.12.1. Cetrimide (CT) as a Cationic Surfactant

Cetrimide (CT), chemically known as cetyltrimethylammonium bromide (CTAB), is a cationic surfactant belonging to the quaternary ammonium compounds (quats). Its chemical formula is $C_{19}H_{42}BrN$, Hydrophobic Tail: Long alkyl chain (C16) derived from acetyl alcohol Hydrophilic Head: Quaternary ammonium group with a positive charge, Properties of Cetrimide Appearance, White or off-white powder or granules, Solubility: Soluble in water and alcohol, pH: Neutral to slightly alkaline, Surface Activity: Reduces surface tension by adsorbing at interfaces (water-air, water-oil), Charge: Positively charged (cationic) in aqueous solutions (See Figure 1.4 for the chemical structure of CT)(42).

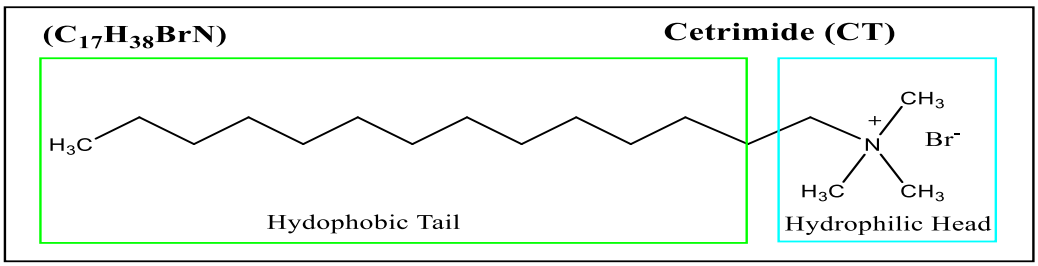

Figure (1.4). Chemical structure of Cetrimide (CT)

1.13. Literature Review

Cobalt ferrite ($CoFe_2O_4$) and its composites have attracted significant attention in recent years due to their unique magnetic, electrical, and catalytic properties. Various synthesis methods have been developed to tailor particle size, morphology, and functionality for diverse applications such as magnetic storage, sensors, wastewater treatment, and biomedical uses. The choice of synthesis method, precursor materials, and composite components greatly influences the final properties of the material. The following table summarizes key studies related to the synthesis of $CoFe_2O_4$ and its composites, highlighting the materials used, synthesis approaches, targeted applications, particle sizes, and corresponding references.

Synthesis Materials	precursors	Synthesis method	Applications	Sizes/ nm	References , and Years
$CoFe_2O_4$	$CoCl_2 \cdot 4H_2O$	Precipitation	magnetic storage	11 and 45	(43) 2010
$CoFe_2O_4$	Co $(NO_3)_2 \cdot 6H_2$ O	combustion	magnetic storage	69.5	(44) 2011
$CoFe_2O_4$	Co $(OH)_2$	combining coprecipitation	Sensors, Data Storage	8.7	(45) 2017
$CoFe_2O_4$	Co $(NO_3)_2 \cdot 6H_2O$	hydrothermal	semiconducting	3.6 to 8.5	(46) 2022
$CoFe_2O_4$	(Fe $(NO_3)_3.9H_2O$)	sol–gel	Biomedical Applications	458	(47) 2023
PANI, $CoFe_2O_4$, TiO2	$CoFe_2O_4$	hydrothermal process and an in-situ polymerization	treatment of wastewater.	400–800	(48) 2013
CF/PANI/rGO	$CoFe_2O_4$	chemical oxidative	Electrocatalysts	29–62	(49)

					2015
$CoFe_2O_4$/rGO/PANI	$CoFe_2O_4$	combustion method, Hummer's method	Wearable Electronics	8.59	(50) 2016
$CoFe_2O_4$, WO3 (PANI)	$CoFe_2O_4$	ionic liquid	Wastewater Treatment		(51) 2021
$CoFe_2O_4$ gCN, PANI	$CoFe_2O_4$	polymerization method.	Industrial Wastewater Treatment		(52) 2022
$CoFe_2O_4$, (PANI), (MWCNT	$CoFe_2O_4$	the sucrose auto-combustion	Industrial Dye Removal		(53) 2024

1.14 The Aim of this Study

This project aims to:

1. Prepare the poly metalate like cobalt ferrite ($CoFe_2O_4$) as an inverse spinel nanomaterial.
2. Prepare the ternary composite $CoFe_2O_4$/ active carbon/ polyaniline.
3. Investigate their characterizations such as X-ray diffraction (XRD), Scan electron Microscopy with energy dispersive X-ray (SEM-EDX), Fourier-transform infrared spectroscopy (FT-IR), N_2 adsorption – desorption.
4. Apply in removal of colored organic pollutant such as the textile dye (direct orange dye), and study the influences such as time of

removal, dose of catalyst, initial pH of solution, temperature, and reuse.

.

Chapter Two The Experimental Part

2. Chemicals and Instruments

2.1. Chemicals

chemicals used in this investigation are presented in Table (2-1); no further purification was necessary.

Table (2.1) Chemicals Used

No.	The chemicals	The company supplied	Purities and percentage %
1.	Absolute ethanol (C_2H_5OH)	Carlo erba, France.	99.9%
2.	Activated carbon	Sigma cheml Co. USA	99%
3.	Ammonia (NH_3)	Country of origin India	99%
4.	Aniline ($C_6H5\ NH_2$)	Country of origin India	99%
5.	Cetrimide (CT) $C_{17}H_{38}BrN$	CDH, India	96-100%
6.	Cobalt nitrate Co $(NO_3)_2.6H_2O$	Sigma cheml Co. USA	99%
7.	Ferric nitrate Fe $(NO_3)_3.6H_2O$	Sigma cheml co. USA.	99%
8.	Hydrochloric acid (HCl)	Sigma Aldrich	37%
9.	Sodium hydroxide (NaOH)	Country of origin India	99%
10.	Direct orange 39 dye	Babel Textile Factory, Iraq	

2.2 Instruments

Table (2.2) describes the instruments that employed in this study, along with their manufacturing companies and locations.

Table (2.2): Employed instruments.

No.	Instruments	Companies	Location
3	Electric Sensitive, Balance.TP-214	Germany Denver	University of Kerbala
2	Brun Auer-Emmett-Teller (BET) analysis	(kyky EM) 320, USA.	Iranian Islamic Republic, Isfahan University
6	Centrifugal	Hettich- Universal II Germany	University of Kerbala, Science college
7	Digital pH meter	OAICTON-2100, Singapore	University of Kerbala, Science college
13	Field Emission-Scanning Electron Microscopy (FE-SEM)	Inspect f 50 ,Fei, Dutch	Alkhora company for general trading -Nano lab
8	Fourier transform infrared (FT-IR)	Shimadzu,8400S Japan	University of Kerbala, Science college
9	Hotplate Magnetic Stirrer	Heido-MrHei-Standard, Germany	University of Kerbala, Science college
4	Scanning Electron Microscopy (SEM)	thermos scientific, Dutch	Alkhora company for general trading -Nano lab
10	The oven	Memmert, Germany.	University of Kerbala, Science college
11	Ultrasonic bath high frequency ≥100 kHz	DAIHAN Scientific, Korea.	University of Kerbala, Science college
12	Ultrasonic bath low frequency = 46 kHz	EASY HOME, turkey	University of Kerbala, Science college
1.	UV-visible spectroscopy.	FAITHFUL-721: China.	University of Kerbala, Science college
5	X-Ray Diffraction Spectroscopy	Lab X- XRD 6000, Shimadzu, Japan	Alkhora company for general trading -Nano lab

2.3. Preparation of Standard Solutions

2.3.1. Preparation of stock solution for direct orange39 dye

A (100mg/L) of dye stock solution was done by dissolving 0.025 g in 250 mL of distilled water. The saris of dye solutions (1– 25) mg/L were produced.

Table (2.3). Calibration curve of Direct orange dye at wavelength 416 nm.

Dye Conc./ ppm	Abs.
1	0.078
5	0.317
10	0.65
15	0.918
20	1.212
25	1.396
30	1.5
50	1.616
60	1.625

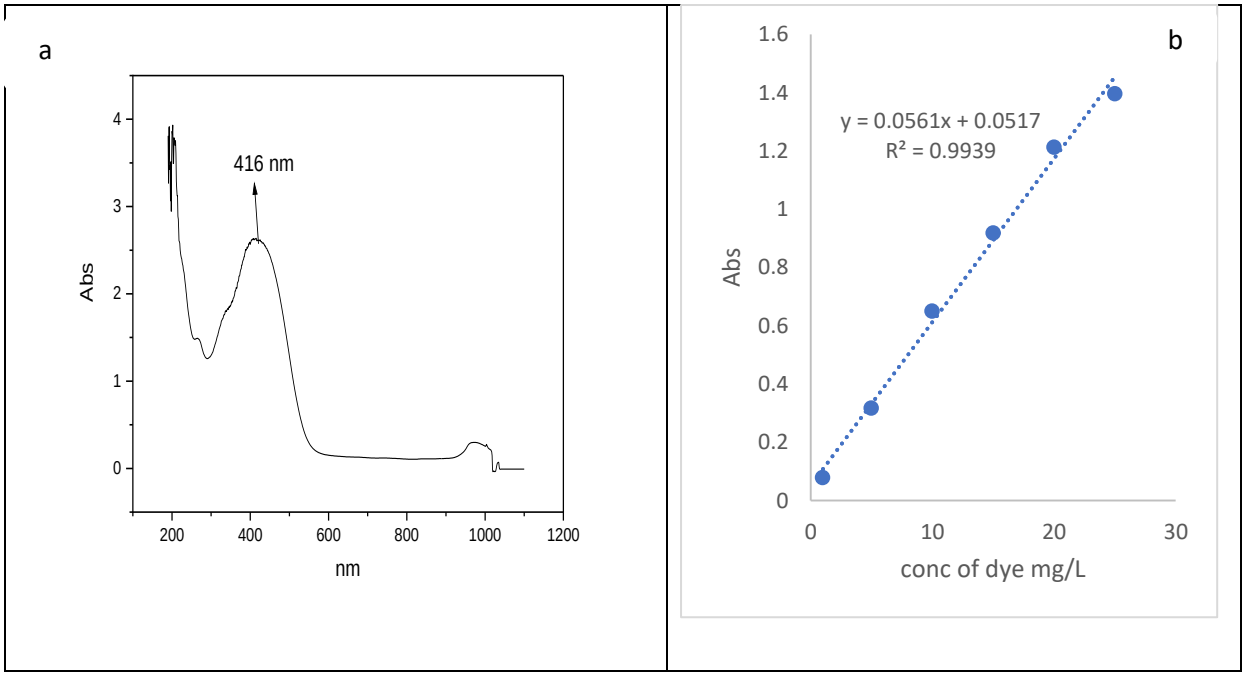

Figure (2.1): (a) UV-Visible Absorption Spectrum for a direct orange 39 dye solution (b)calibration curve for the determination of direct orange 39 dye in aqueous solution at 416 nm wavelength

2.3.2. Preparation of 3 M of Acid Solutions

A 25 mL volumetric flask containing half cold distilled water was filled with precisely 6.25 mL of strong hydrochloric acid (1.18 g/mL, 35%, and 36.46 g/mol), and the volume was carefully adjusted by cold distilling to 25 mL.

2.3.3. Preparation of oxidant solution

9.31 g of oxidant solution ammonium persulfate (APS) was dissolved in 50 mL of aqueous solution with 1 M HCl to create the oxidant solution (APS).

2.3.4. Preparation of Sodium hydroxide (1 M) Solutions

This solution was prepared by dissolving 2 g of NaOH in less amount of distilled water, then transferred to a volumetric flask size 50 mL, and added D.W to reach the mark.

2.4. Preparation of Cobalt Ferrite Nanoparticles

The bare $CoFe_2O_4$ nanoparticles were synthesized in precipitation method in presence of the positive surfactant as a template, stabilizer and capping agent. Exact 13.9 g of ferric nitrate Fe $(NO_3)_3.6H_2O$ was dissolved in 200 mL of distilled water, in other container, 4.14 g of cobalt nitrate $CO(NO_3)_2.6H_2O$ was dissolved in 200 mL of distilled water. The cobalt solution was gradually dropped into iron solution with stirring under conditions of room temperature. Subsequently, 1 g of the surfactant citermide (CT) was added to mixture with stirring ten minutes. Conc. ammonia solution (5 mL) was added. slowly dropwise through the burette

into this stirring until pH of the solution was reached between 9.5 and 10. This mixture was heating and stirred at 75-80 ^{o}C for 1h, a black semi-solid material was obtained, this material was filtered and washed with distilled water and ethanol. The produced precipitate was dried using oven for setting at 100°C for 2 hours, and then the material was burned at 300°C for2 h., Figure (2-1) provided an explanation of the synthesis steps.

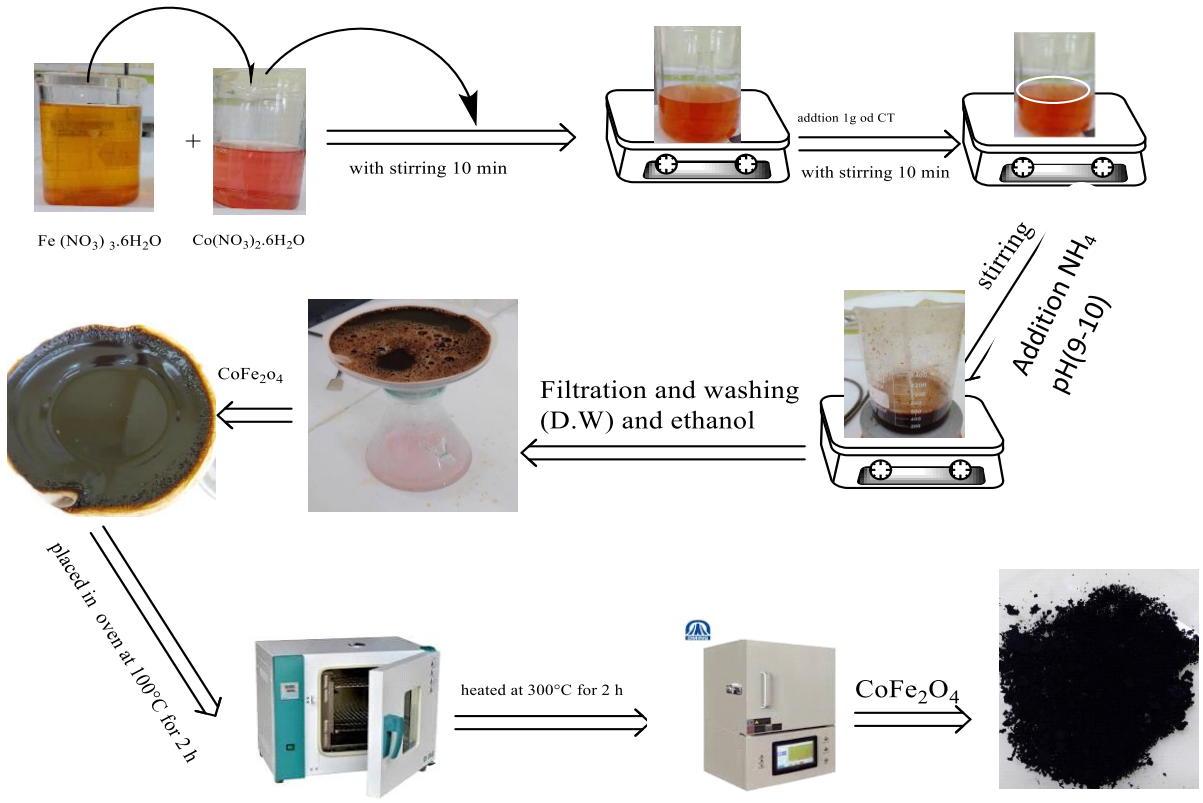

Figure 2.2. Diagrammatic representation of the procedures of cobalt ferrite nanoparticles

2.4.1. Preparation of Ternary Composited

Chemical oxidation polymerization was used to create the $CoFe_2O_4$/AC/ PANI nanocomposite, with HCl and ammonium persulfate (APS) acting as dopants and oxidants, respectively. The oxidant solution of Ammonium persulfate (APS) was prepared by dissolving 9.31 grams of APS in 50 milliliters of 1 M HCl solution [11].

Exact (1 g) of $CoFe_2O_4$ and (1 g) active carbon (Ac) as ratio (1:1) were added to aniline in ice bath at 0 ^oC, which made beforehand (5 g of aniline, with a density of 1.33 (g/cm^3) in 82 mL of 1 M HCl solution) and mixed using ultra-sonication for 10 min. the final mixture was mixed together in ice bath for 1h at 0-2 ^oC. In order to fully combined PANI with $CoFe_2O_4$ and AC, oxidant solution of (APS) must gradually add (at ten drops per minute) as a molar ratio of 3:1 using separating funnel to final solution in ice bath at 1-2 ^oC for 1h. This mention conditions were essentially to polymerize the monomers of aniline at 1 to 2 ^oC[11], and change the solution color from dark brown to black suspension. The polymerization reaction was then carried out for an entire night, and the color of the solution was modified from black to dark black- green (oily color) confirming the PANI nanocomposite was produced. The suspension of $CoFe_2O_4$/AC/ PANI nanocomposite was filtered by Buchner funnel, then washed with fresh distilled water. The product was dried under vacuum. The steps of ternary composite synthesis were performed as seen in figure (2.3) .

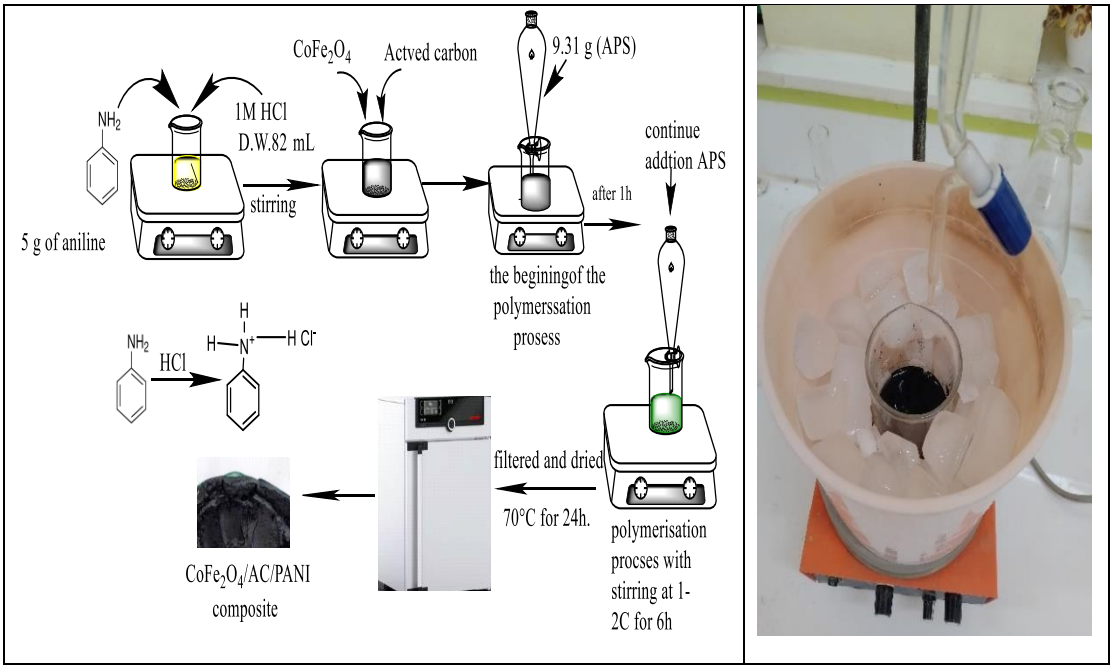

Figure (2-3). A schematic diagram of the stages involved in producing ternary composite nanoparticles.

2.5. Characterization of Spinal $CoFe_2O_4$ and composited.

2.5.1. Fourier transform infrared (FT-IR) Spectroscopy

This analysis was performed using KBr pellet method at room temperature, (FT-IR) spectra were recorded on a Perkin Elmer Instrument Spectra FTIR-2 to determine the functional groups in cobalt ferrite and its composite.

2.5.2. Spectroscopy using X-Ray Diffraction (XRD)

The mean crystal sizes (D) of each sample were determined using X-ray data and Scherer's equation (eq. 2-1) [52, 53]. The Shimadzu Lab-XRD 6000 equipment were used to record the diffractograms. The target source of Cu wavelength was 1.540 60 Å, the voltage was 40.0 kV with 30 mA current, the speed was 12.0000 deg/min, and the scan angle was 20-80.

$$D = \frac{k\,\lambda}{\beta\,\mathrm{Cos}\,\theta} \qquad \ldots. (2\text{-}1)$$

Here, θ is the Bragg angle, λ is the X-ray wave length (1.5406 nm), β1/2 is the Full Width Half-maxima (FWHM), D is the particle's crystallite size, and k is the Scherer constant, which ranges from 0.84 to 0.94 (54).

2.5.3. Scanning Electron Microscopy (SEM)

The properties of the surface morphology of the prepared nanomaterial were revealed via the application of the field emission scanning electron microscopy (SEM) technique. the specimens were examined at 60 kx magnification and an electron high tension EHT of 10 kV in a Zeiss, Germany, SEM (55).

2.5.4. **Energy Dispersive X-ray Analysis (EDX-Elemental).**

This method provides an information about elemental compositions. Each element's spectrum is acquired by irradiating the sample's atoms with an electron beam. There is a certain similarity between this method and scanning electron microscopy(56).

2.5.5. N_2 Adsorption - desorption isotherm Analysis.

BET analysis was conducted to determine the specific surface area, total pore volume, and average pore diameter of cobalt ferrite and composite nanoparticles. These parameters are critical for understanding the surface properties and potential catalytic activity of the nanoparticles.

2.6. Some Factors Affecting the Dye Removal Process

2.6.1. Equilibrium Time

The best contact time can be investigated to find the achieved equilibrium between the adsorbent surface (synthesis catalysts) and the adsorbant(dye) at ranged from 10 to 60 min. For dye concentration of 5 mg/L in 25 mL with a surface weight of 0.025g at 298 K, the absorbance of the dye residue in solutions can be measured at the maximum wavelength 416nm (57).The adsorption constant, adsorption capacity and percentage of removal were measured by the following equation(2.2), **(2.3),** (2.4)(58)(59)(60)

$$k_{d=}\frac{C_{ads}}{C_e} \quad \ldots (2.2)$$

$$\boldsymbol{Qe} = \frac{\boldsymbol{v(C_o - C_e)}}{\boldsymbol{m}} \quad \textbf{.... (2.3)}$$

$$\mathbf{R_{emoval}\ \%} = \frac{\mathbf{Co - Ce}}{\mathbf{Co}} * \mathbf{100}\% \quad \ldots. (2.4)$$

2.6.2. Effect of the Weight of Surface Adsorbent

The changing in the weight of adsorbent surface has an influence on adsorption. Therefore, it was examined with dye concentrations of 5 mg/L in 25 mL and different weights of the adsorbent surfaces ranging (0.1, 0.2, 0.3,0.4) g, followed by a shaking period of (10 to 60) minutes at 298K. The adsorption constant, adsorption capacity and percentage of removal were also determined, as mention in paragraph 2.6.1 (61).

2.6.3. Effect of concentration

Different samples were made by combining 25 mL of direct orange solution at different concentrations (5, 10, 15,) mg. mL^{-1} with 0.3 g of the prepared cobalt ferrite particles in order to ascertain the concentration necessary for adsorption. After being agitated for 90 minutes at a speed of 140 t/min, kept the temperature at 25℃. The samples were filtered. The supernatants' absorbance was then measured with a UV-Vis spectrophotometer. as mentioned in paragraph 2.6.1.

2.6.4. Effect of pH on the dye

The acidity function is a vital parameter that direct effect on the removal rate and adsorption process, this parameter was performed range (pH = 4,5,6,7,9, and 11) at dye concentrations 5 mg/L in 25 mL and optimum dose of catalyst at 298 K. The adsorption constant, adsorption capacity and percentage of removal were also found, as mentioned in paragraph 2.6.1

2.6.5. Effect of Temperature

The study of temperature on the adsorption process is essential parameter, hence, the temperature range (278 - 323) K was applied to find

the adsorption capacity, adsorption constant and percentage of removal were also calculated, as mentioned in paragraph 2.6.1.

2.7. Reusability of cobalt ferrite and composite Nanoparticles

Cobalt ferrite and composite nanoparticles were reused numerous times, and their performance efficiency and adsorption capacity were investigated. The process was carried out using 0.3g cobalt ferrite and composite and 5 mg. L^{-1} detect orange dye concentration in 25 mL under optimal conditions of 25°C and pH 6. After that, it was placed in the shaker for 45 minutes before being transferred to the centrifuge for separation and measurement of the absorbance of the prepared solutions. Finally, the solutions were filtered and the precipitate was reused again. This procedure was carried out five times. The nanoparticles demonstrated a significant adsorption capacity even after multiple cycles in the composite.

2.8. Equilibrium Isotherm Modeling

Decolonization isotherms were found by adding 0.3g $CoFe_2O_4$ to different dye concentrations (ranging from 5 to 15 mg/L) and temperatures (ranging from 10 to 25 oC) with the appropriate pH adjustment. Experimental data at equilibrium concentrations of dye adsorbed (qe) on the adsorbent (cobalt ferrite and composite) and dye concentration in solution (Ce) at constant pH and temperature levels were used to describe the ideal isotherm model. The Langmuir and Freundlich equations were expressed in linear form to describe the equilibrium data (Table 2.4). The applicability of these equations was compared using correlation coefficients (R2). (62).

Table (2.4): Different isotherm models used in this study and their linear forms

Isotherm	Nonlinear form	Linear form	Plot
Langmuir	$q_e = \frac{KLCe}{1+KLCe}$	$\frac{C_e}{q_e} = \frac{1}{k_L \times q_m} + \frac{C_e}{q_m}$ **(2.5)** (63)	$\frac{1}{qe}$ VS $\frac{1}{Ce}$
Freundlich	$q_e = K_F\, Ce^{1/n}$	$\boldsymbol{\log q_e = \log k_F} + \frac{1}{n}\boldsymbol{\log C_e}$ $(\mathbf{2.6})$ (64)	Log q_e VS log C_e

2.9. Adsorption Kinetics

To investigate the adsorption mechanism of direct orange dye on the surface of $CoFe_2O_4$, and PANI/AC/$CoFe_2O_4$, two kinetic models, pseudo-first-order and pseudo second-order kinetic model, were tested to find the best fitted model for the experimental data.

The pseudo-first-order Lagergren equation is given by (65)

$$log(qe - qt) = logqe - \frac{k1t}{2.303} \qquad (2.7)$$

where k_1 is the pseudo-first-order rate constant (min^{-1}), q_e and q_t are the amounts of dye adsorbed (mgg^{-1}) at equilibrium and at time t (min).

The pseudo-second-order model can be expressed as (66)

$$\frac{t}{qt} = \frac{1}{k2q2e} + \frac{1}{qt} \qquad (2.8)$$

where k_2 ($gmg^{-1}\,min^{-1}$) is the rate constant of the pseudo-second order adsorption. The initial adsorption rate in the pseudo-second order kinetic model is $h = tq^2_e$

Chapter Three

Results and Discussion

3. Chapter Three: Results and Discussion

3.2. Characterization.

The FT-IR, (XRD), (SEM), (EDX), and N_2 adsorption- desorption analysis was employed to assess the created $CoFe_2O_4$ nano powder and its composite.

3.2.1. FT-IR Spectral Analysis

Based on FTIR analysis in figure 3.1, the black spectrum for $CoFe_2O_4$ detects the stretching vibrations of tetrahedral and octahedral metal oxygen bonding are represented by two stretching frequencies that are detected between 400 and 600 cm^{-1}. The strong stretching vibration peak at a higher frequency of 582.52 cm^{-1} illustrates the tetrahedral sites of (Fe–O), whereas the stretching vibrations of the metal complex (Co–O–Fe) in octahedral sites appears at a lower peak frequency of 470.36 cm^{-1} (67). These two peaks' existence validates $CoFe_2O_4$ inverse spinel phase (68). The absorption band at 3124 cm^{-1} was identified as the O-H stretching mode (69) The FT-IR spectrum of the PANI is displayed spectrum. The region of 1528 to 794 cm^{-1} is where the distinctive peaks of PANI are found. The typical C=C stretching of the quinoid and benzenoid rings is responsible for the absorbance peaks at 1572 and 1492 cm^{-1}, whilst the C-N stretching of the secondary aromatic amine is responsible for the band seen at 1295 cm^{-1}. The in-plane bending modes of aromatic C-H are often detected in the range of 1108-1203 cm^{-1}, with a peak at 1149 cm^{-1} and an out-of-plane deformation at 794 cm^{-1}. These vibrational modes provide critical information about the structural characteristics and electronic properties of PANI (70). Understanding these peaks allows researchers to manipulate the material for various applications, including sensors and conductive polymers. Furthermore, the analysis of these vibrational modes can lead to insights into the polymer's conductivity and stability under different environmental conditions. By correlating the spectroscopic data with the material's

performance, scientists can optimize PANI for enhanced functionality in electronic devices (71) It is worthily mentioned that their intensity and location of the characteristic peaks of PANI change, indicating some chemical interaction between $CoFe_2O_4$ and PANI. In red spectrum, the presence of 1513.08 cm^{-1} peak in $CoFe_2O_4$/AC/ PANI corresponds to form new bonds due to the combination of three components because this peak does not appear in $CoFe_2O_4$ (black spectrum) this peak may be due to the C=N vibrations affected by the interference of AC with PANI. The peak at 786.98 cm^{-1} in spectrum of the ternary compound is associated with the interactions between PAN, $CoFe_2O_4$ and activated carbon. Indeed, the sharp peaks at 470.65 cm^{-1} and 1513.08 $cm^{-1}$are related with the vibrations of Co–O–Fe in octahedral sites.(72).

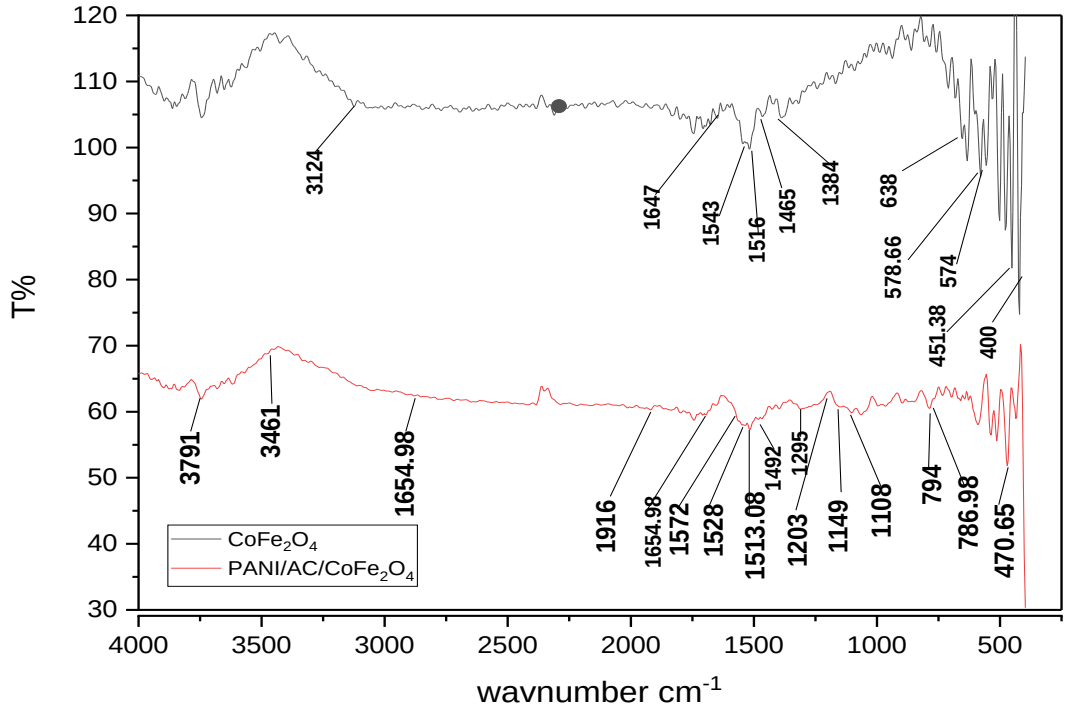

Figure (3.1). The FT-IR spectra of $CoFe_2O_4$ and composite synthesis.

3.2.2. X-ray diffraction (XRD) analysis

The X-ray diffraction patterns of $CoFe_2O_4$ have been studied. The analysis was carried out under exact parameters, which included an 8-mA current, a 40 kV voltage, a step size of 0.0110, at a step rate of 1 s per step. It is noteworthy that no additional peaks were found in the XRD patterns, suggesting the absence of contaminants. Bragg reflections were measured between 7.0054 and 79.9904 to ensure sample purity. The X-ray diffraction profile provided vital information about the synthesized powder sample's qualitative and quantitative phases, as well as its preferred orientation. figure 3.2 black line) illustrates the X-ray diffraction structure of $CoFe_2O_4$, having The XRD analysis of (black line) conformed that the face centered cubic spinel lattice of $CoFe_2O_4$ is synthesis according to the diffraction peaks around 2θ =18, 30.45, 35.88, 43.56, 54.17, are attributed to the (111) (220), (311), (222) and (400), respectively (JCPDS -22-1086)(67)(73). The absence of any discernible impurity phase was one of the synthesized powders' noteworthy characteristics. The cobalt ferrite nanoparticles in the sample displayed peaks that matched the location of a cubic unit cell, suggesting an inverse spinel structure. The crystallite size in $CoFe_2O_4$ was determined to be 31.83 nm using statistical analysis and the Debye Scherer equation (2.1) [80]. The $CoFe_2O_4$ /AC/ PANI sample contained all of the XRD peaks linked to AC, $CoFe_2O_4$ and PANI when comparing the functional groups of the AC, $CoFe_2O_4$, and PANI samples with the sample of the $CoFe_2O_4$ /AC/ PANI composite. The structure of the $CoFe_2O_4$ /AC/ PANI was thus preserved without changes in the crystal planes, with the exception of minor shifts in positions and variations in the intensities of the associated XRD peaks in comparison to those found in the individual active carbon, $CoFe_2O_4$, and PANI samples. These thus showed that PANI had successfully interacted with AC and $CoFe_2O_4$ In conclusion, our findings support the FTIR data by confirming that PANI was successfully applied to active carbon

and $CoFe_2O_4$. The ternary complex's crystalline size(36nm) was determined by equation .(54)

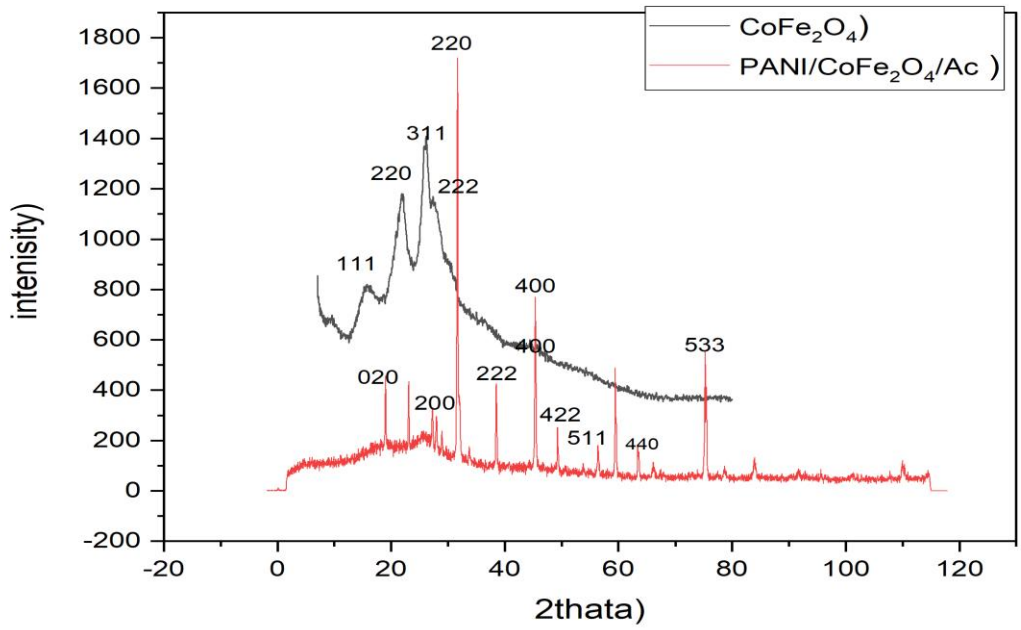

Figure (3.2). **(XRD) analysis** of $CoFe_2O_4$ and composite synthesis.

3.2.3. Scanning Electron Microscopy (SEM) Analysis

This SEM image (a) exhibits nanoparticles with size measures in nanometers, revealing the average particle sizes of a $CoFe_2O_4$ sample. The picture labels several nanoparticle sizes, ranged (33.03 and 41.35) nm. These results are acceptable with polycrystalline nanoparticle architectures. The particles' size and shape are reasonably uniform, indicating a homogeneous synthesis process. Materials such as $CoFe_2O_4$(74)(75) in (figure 3.3 (a) are known for their virtually texture-like particles. The particle sizes in image b are showed from 29.34 nm to 49.90 nm with agglomerated as layers. These particle sizes are increased compared with their for CoF_2O_4 (76). Because of the differing electron penetrability, the black region shows the presence of magnetic $CoFe_2O_4$ particles in the composite, whereas the light-colored region represents activated carbon(65).

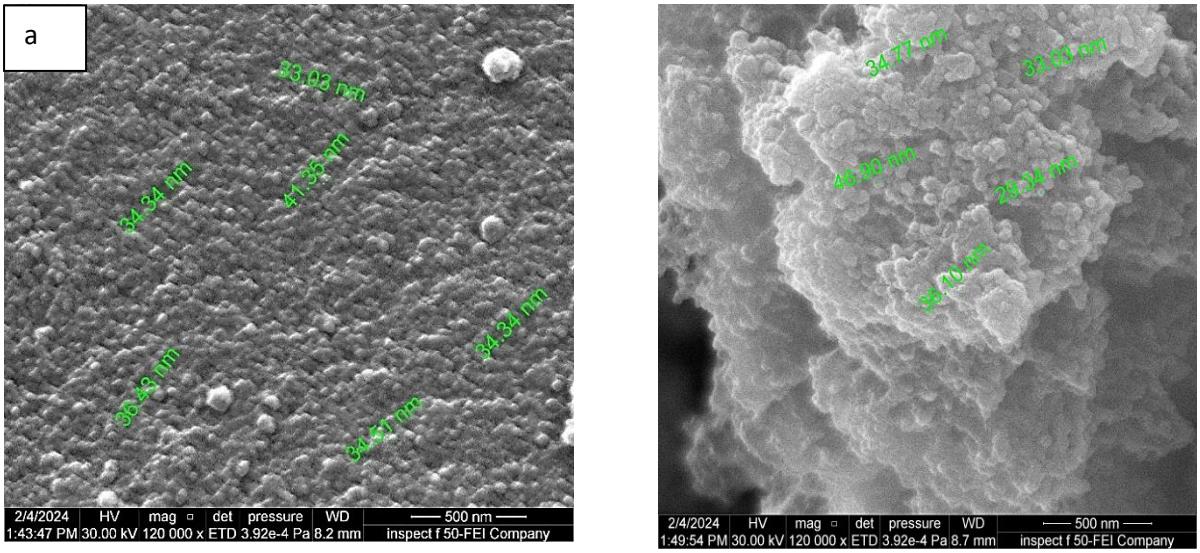

Figure (3.3): The scanning electron microscope (SEM) spectrum of (a) cobalt ferrite, (b) composite

3.2.4. EDAX analysis for cobalt ferrite and composite.

The EDX spectrum for cobalt ferrite ($CoFe_2O_4$) (Figure 3.4a) confirms the formation of cobalt ferrite nanoparticles with a distinct elemental composition of cobalt, iron, and oxygen. The absence of additional elemental peaks suggests that the sample is free from impurities. Furthermore, the analysis reveals the expected stoichiometric ratio of cobalt, iron, and oxygen, characteristic of cobalt ferrite.

In contrast, the EDX spectrum for the composite material (Figure 3.4b) reveals a different elemental composition, including carbon, nitrogen, oxygen, cobalt, and iron Compared to cobalt ferrite ($CoFe_2O_4$), The carbon element comes from polyaniline which is formed by the molecular formula $C_6H_5NH_2$.

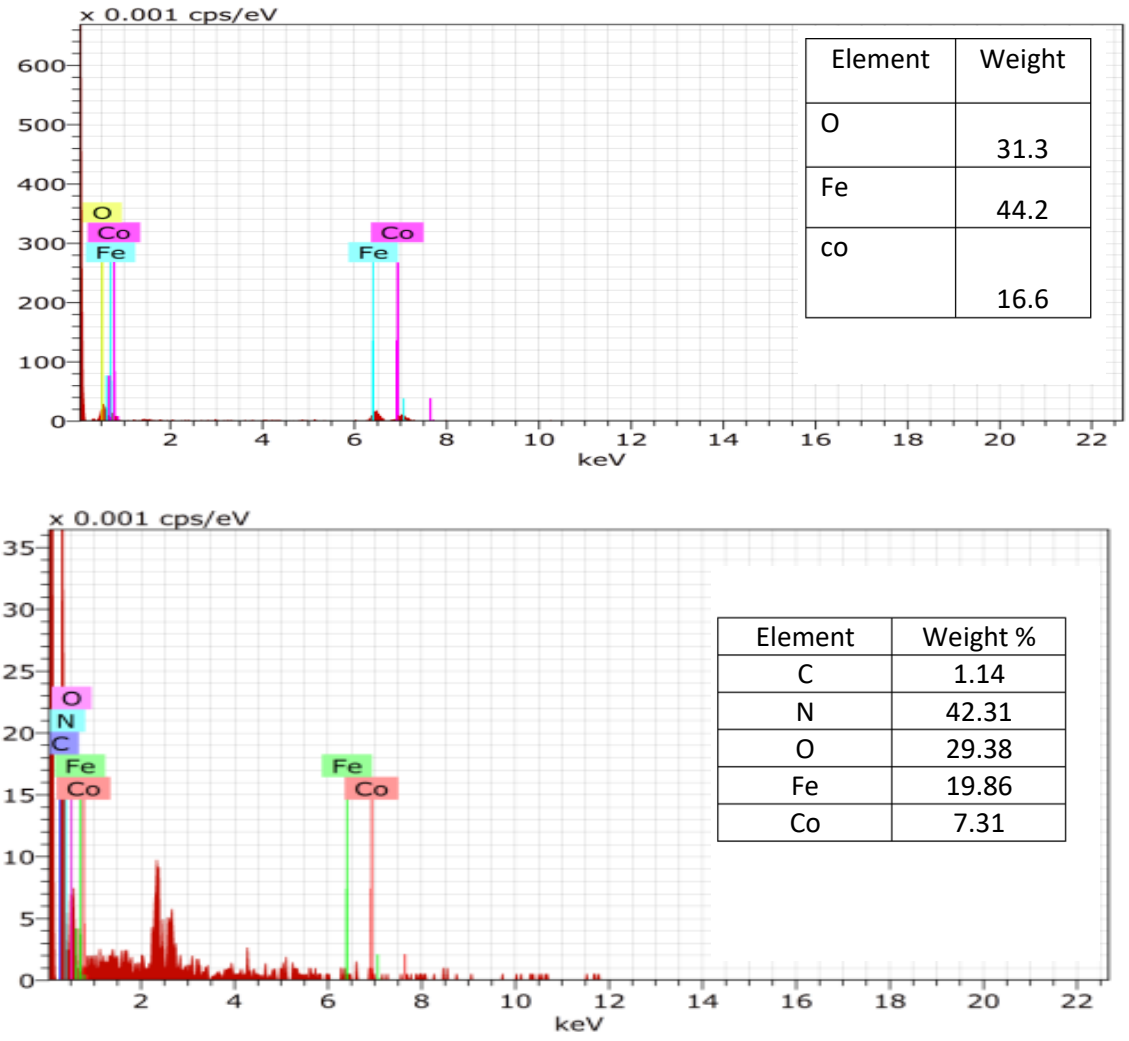

Figure (3.4): EDX spectrum **of (a) $CoFe_2O_4$ (b)** PAIN/AC/Fe_2O_4

3.2.5. N_2 Adsorption-Desorption isotherm analysis for cobalt ferrite and composite

The BET surface areas and pore size distribution of all the samples were obtained from the nitrogen adsorption-desorption isotherm. From BET plots, the surface parameters for each of the samples of pure, $CoFe_2O_4$ and PAIN/AC/$CoFe_2O_4$ nanocomposite have presented. The hysteresis loops in Fig.(3.5), are in agreement with Adsorption isotherms type IV, and the hysteresis loop was demonstrated in the relative pressure (P/P_0) range of 0.3~1.0, belonging to type H3(77) (78). The expected pores for $CoFe_2O_4$ and PAIN/AC/$CoFe_2O_4$ nanocomposite are open with semi-spherical shape and closed with spherical shape, respectively(79). The table

(3.1) demonstrates, the specific surface area, and mean pore diameters of the $CoFe_2O_4$ and PANI/AC/$CoFe_2O_4$ nanocomposite are 8.9064 m^2g^{-1}, 22.662 nm and 54.118 m^2/g^{-1}, and 9.4355nm, respectively. That confirmed increase in surface area after synthesis of composite and that the pores exhibited are mesoporous characteristics, this porosity enhances the accessibility of reactants to the active sites on the nanoparticle surface, making them suitable for various applications such as catalysis adsorption [80]. Total pore volume ($cm^3.g^{-1}$) are approximately 0.1277 and 0.05046 for $CoFe_2O_4$ and PAIN/AC/$CoFe_2O_4$, respectively, which confirmed that the structures of both samples contained micropores (80)

Table (3.1) N_2 Adsorption - desorption isotherm (BET) Analysis for $CoFe_2O_4$ and PAIN/AC/$CoFe_2O_4$.

Compounds	**BET surface area ($m^2.g^{-1}$)**	**Total pore volume ($cm^3.g^{-1}$)**	**Average pore size (nm)**
$CoFe_2O_4$	8.9064	0.05046	22.662
PAIN/AC/$CoFe_2O_4$	54.118	0.1277	9.4355

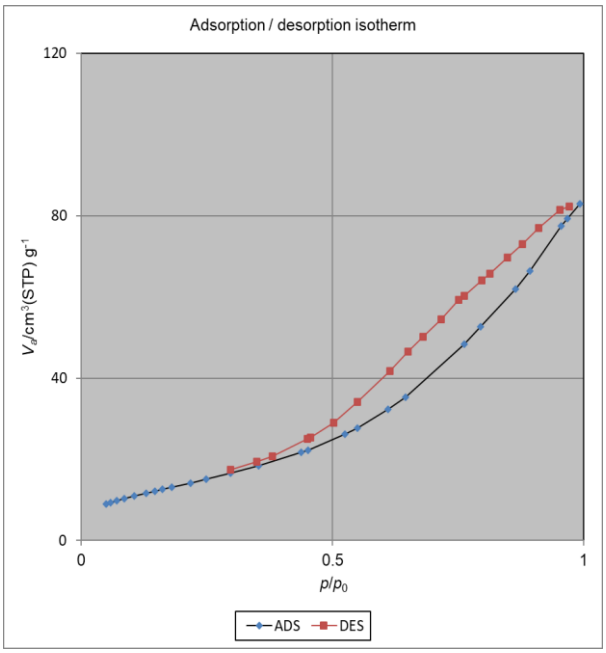

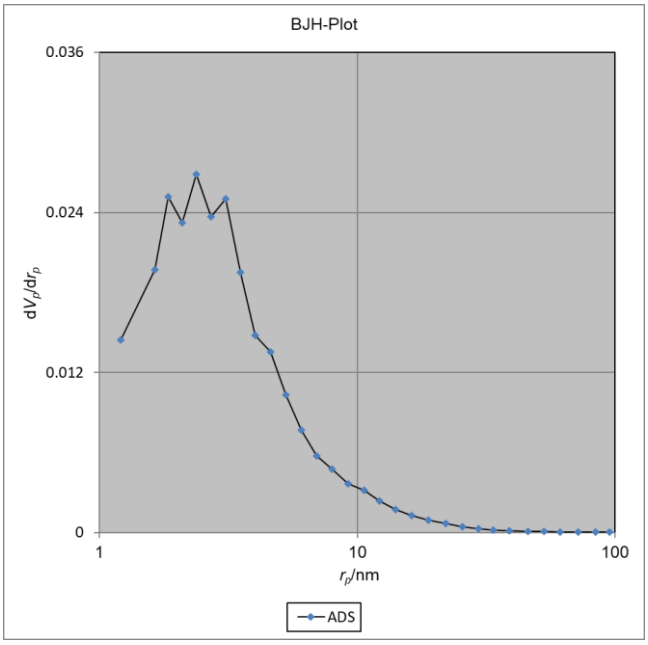

Figure (3.5). N_2 Adsorption - desorption isotherm (BET) Analysis of $CoFe_2O_4$.

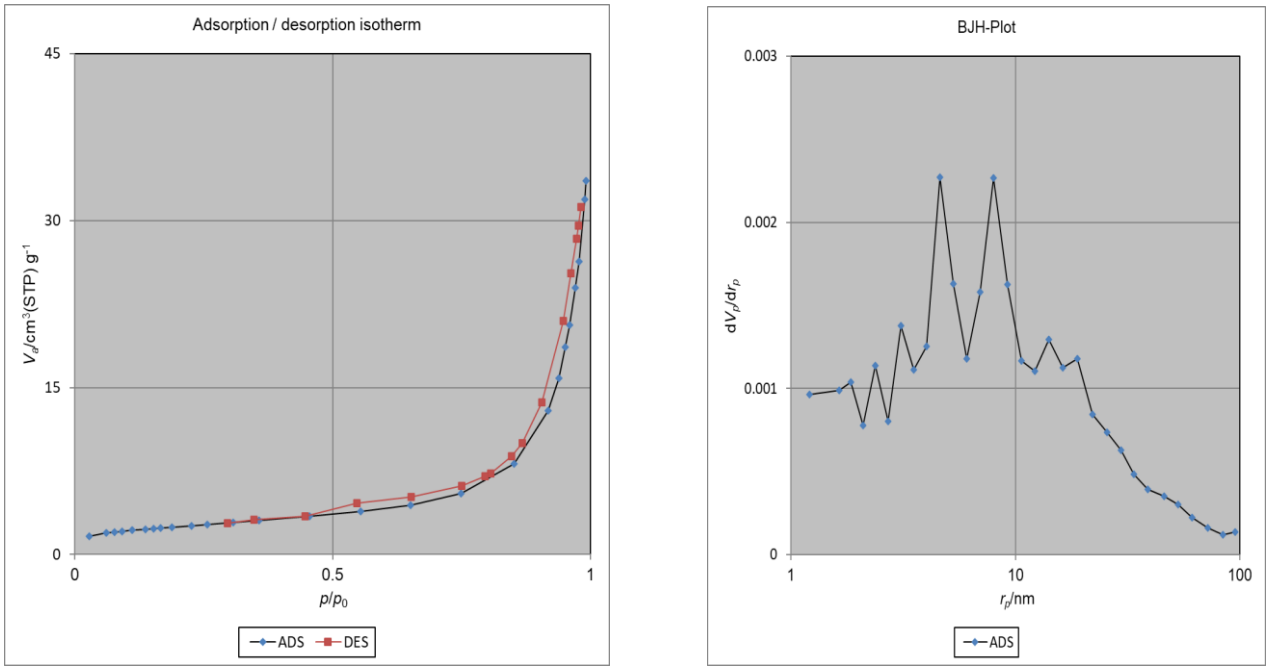

Figure (3.6). N_2 Adsorption - desorption isotherm (BET) Analysis of composite

3.3. Study Factors influencing on Removal of direct orange Dyes.

This section comprises several experiments that could highlight all of the elements influencing the use of $COFe_2O_4$ NP for the removal of direct orange dye pollution from water. The work also contains adsorption isotherms, theoretical models that characterize them, and the thermodynamics of the adsorption process.

3.3.1. Equilibrium Time of Adsorption System.

A concentration of 5 mg/L in direct orange dye and a surface weight of 0.3 g for ($CoFe_2O_4$) and ternary composite they were added in order to determine the optimum time required to reach for equilibrium between the adsorbent surface and the adsorbate(dye). At lab temperature (298K), shaking every 10, 15, 30, 45, and 60 minutes. After that, the absorbance of residue dye in solution was measured at 416 nm. Because it enters an equilibrium state when the dye has individually occupied all of the active sites in the adsorption medium, the data displayed in Figure (3.7) and Table(3.2).

Table (3.2): Removal percentages of direct orange dye from aqueous solutions using $CoFe_2O_4$ and PANI AC $CoFe_2O_4$ at different times (298k)

$(\boldsymbol{R}\ \%) = \frac{\boldsymbol{C0 - Ce}}{\boldsymbol{C0}} \times \mathbf{100}$		
Time/min.	$CoFe_2O_4$ (%)	Composite (%)
15	27.33447	25.97623
30	37.18166	62.64856
45	69.43973	95.24618
60	64.00679	86.75722

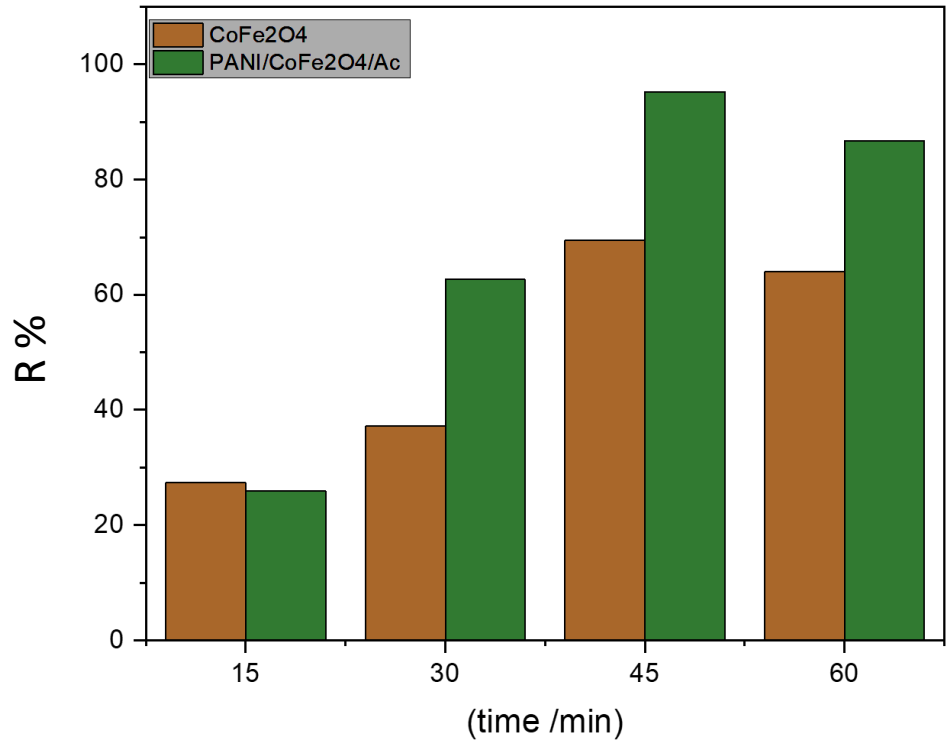

Figure (3.7): Effect of equilibrium time on direct orange dye removal efficiency percentage **(**conditions: pH 6; dosage= 0.3 g**;** concentration of dye 5 mg/L**,** V=50 mL; time= **(**15-60) min and T=298 K)

3.3.2. Effect of the Weight of Surface Adsorbent

Variations in the adsorbent surface's weight have an impact on the direct orange dye's removal, as shown in figure 3.8 and Table 3.3. The E removal % of dye using $CoFe_2O_4$ and its composite are found to be maximum value at weight of 0.3 g, then has no effect on the surface since it is saturated with the adsorbate. Consequently, the optimal adsorption rate of the dye was attained. This achievement highlighted the efficiency of the adsorption process under the specific conditions tested. Further studies could explore the impact of different variables to enhance the overall performance and applicability of the method.

The higher percentage of dye removal (%) for using the composite is more than it values when using $CoFe_2O_4$ NP, which due to a bigger surface area with more active sites accessible for adsorption resulting in the adsorbing surface weight increase (81).

Table (3.3) effect of adsorbent dose on adsorption of direct orange dye on $CoFe_2O_4$NPsand composite.

$(\boldsymbol{R}\ \%) = \frac{\boldsymbol{C0 - Ce}}{\boldsymbol{C0}} \times \mathbf{100}$		
Wt. (g)	$CoFe_2O_4$	composite
0.1	28.353	62.648
0.2	69.439	80.475
0.3	**82.342**	95.678
0.4	75.125	87.328

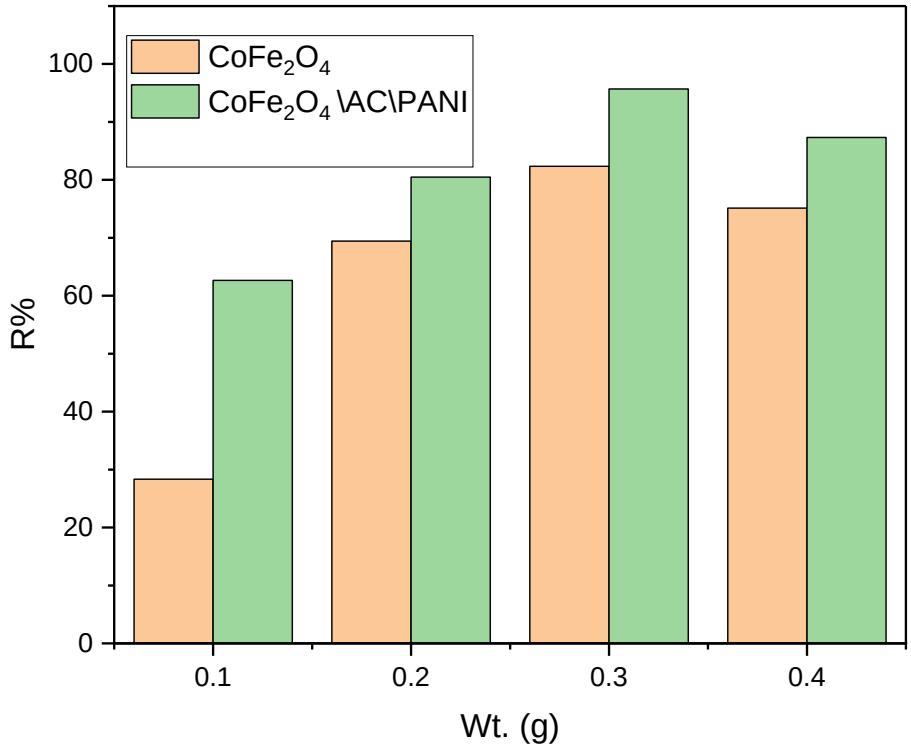

Figure (3.8): Effecting of surface weight of $CoFe_2O_4$ and composite on clearance rate of direct orange dye (conditions: pH 6; concentration of dye 5 mg/L, V=50 mL; time=45 min; dosage 0.1-0.4 g and T=298 K)

3.3.3. Effect of Concentration

The composite outperforms $CoFe_2O_4$ in all cases, particularly at lower concentrations, due to its superior surface properties and higher availability of active adsorption sites of composite, as shown in Figure 3.9 and Table 3.4. However, as the dye concentration increases, the performance of removal for both materials decreases because the adsorption sites become fastly saturated for $CoFe_2O_4$, but for using composite with 5 mg. L^{-1} of dye. the value still retainins a relatively better efficiency (95 %), due to high surface area(82).

$$(R\,\%) = \frac{C0 - Ce}{C0} \times 100$$

Table (3.4) Effect of adsorbent concentration on adsorption of direct orange dye on $CoFe_2O_4$NPsand composite

Conc. mg. L^{-1}	$CoFe_2O_4$	Composite
5	82.34295	95.2461
10	35.0180	80.4753
15	0.8488	57.3288

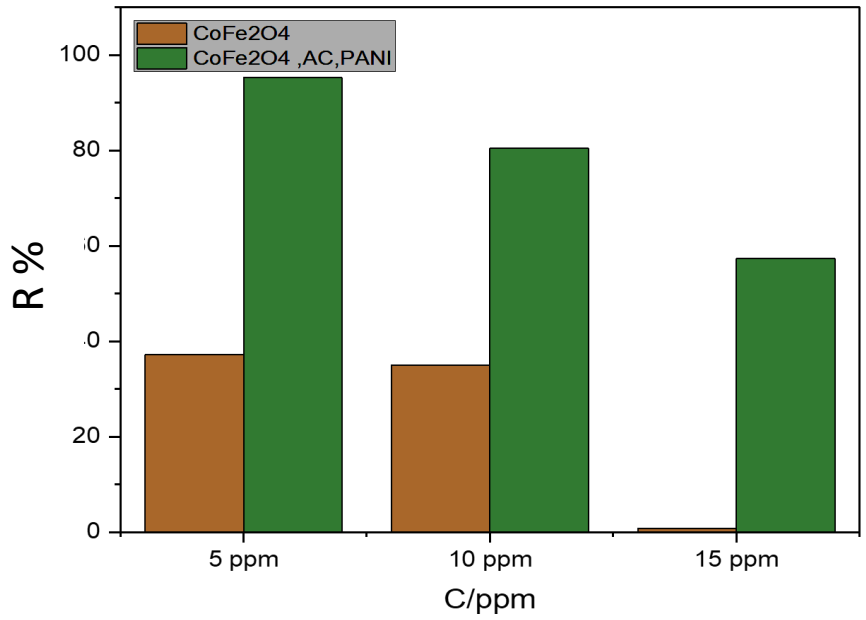

Figure (3.9). Effect of conc on adsorption of direct orange dyes on $CoFe_2O_4$ and composite (conditions: pH 6; dosage= 0.3 g**;** V=50 mL; time=45 min; concentration of dye= (5-15) mg/Land T=298 K)

3.3.4. Effect of pH

The composite shows higher and more stable dye removal efficiency across a wide pH range, making it more effective than pure $CoFe_2O_4$ for dye removal applications.

Table (3.5). The effect of pH on direct orange dye adsorption on $CoFe_2O_4$ and composite.

$(R\ \%) = \frac{C0 - Ce}{C0} \times 100$		
pH	$CoFe_2O_4$	composite
4	8.658744	47.36842
5	57.55518	71.13752
6	82.34295	95.24618
7	29.71138	72.1562
9	23.9388	68.76061

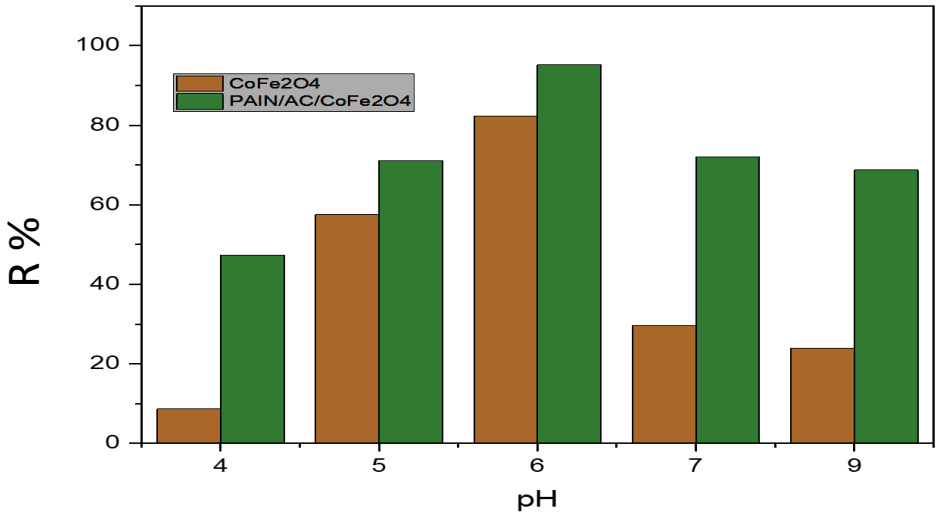

Figure (3.10) Effect of pH on adsorption of direct orange dyes on $CoFe_2O_4$ and composite (conditions: pH 9-4; dosage= 0.3 **g;** concentration of dye 5 mg/L**,** V=50 mL; time=45 min and T=298 K)

3.3.5. Effect of temperature

Both the dye's structure and how well nanoparticles remove it can be affected by temperature. Thus, the effects of temperature ranging from 283 to 298 K on the dye used, the incubation time of 45 minutes, the percentage of E elimination, and qe were assessed. The removal values increase as the temperature in the composite

increases, as shown by the data in figure 3.11, table (3.6). This behavior demonstrates how dyes become more mobile and have larger kinetic energies as the temperature rises, which facilitates their ability to reach active site surfaces. composite and given maximum $E_{removal}$ % that equal to 95.24. while in the case of $CoFe_2O_4$ it is the opposite, as the temperature increases, the removal decreases, as is stated in the figure and table mentioned in a previous paragraph, The reason is due to the occurrence of a rearrangement of cobalt ferrite atoms on a surface at high temperatures, and thus a decrease in the surface area. This means that there are fewer active sites on the surface to which the dye molecules are attached.(83), The negative value of activation energy indicates the uptake of dye from solution is a fast reaction, moreover that may be interpreted to find multi-step binding on $CoFe_2O_4$ surface because it contains two different ions with different oxidation states and they demonstrate two different hybridization (tetrahedral and octahedral) in FT-IR analysis.

Table (3.6) The percentages of direct orange dye removal from aqueous solutions at different temperatures.

$(\boldsymbol{R}\ \%) = \frac{C0 - Ce}{C0} \times 100$		
t/ ^{o}C	$CoFe_2O_4$	composite
10	97.28353	59.25297
15	87.09677	63.32767
20	86.0781	79.62649
25	82.34295	95.24618

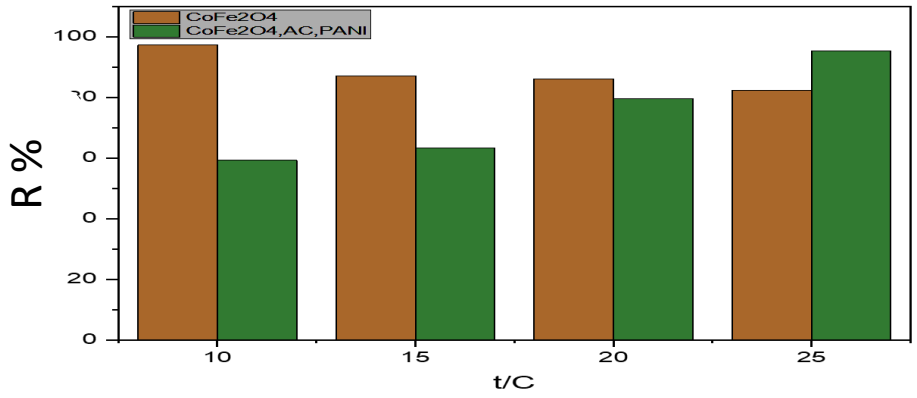

Figure (3.11). Effect of temperature on removal dye by cobalt ferrite and composite (NP) effectiveness. **(**conditions: pH 6; dosage**=** 0.3 **g;** concentration of dye 5 mg/L**,** V=50 mL; time=45 min and temperature = (283-298 k)

Thermodynamic characteristics are crucial for analyzing the kind of adsorption process that took place on any solid surface. The sorption distribution coefficient (kd) was first calculated using equation (1.4). Thermodynamic factors were determined using equations 1-3 to 1-7. Based on the findings in figures 3.10 and 3.11. The results can be comparison between cobalt ferrite and composite in table 3.2.

Table (3.7): The kinetic and Thermodynamic Parameters for direct orange dye adsorption on $CoFe_2O_4$ and composite surface at (278-303) K.

Adsorbates	**(1000/T)**	**Ln k_d**	**ΔH^o kJ mol^{-1}**	**ΔS^o kJ mol^{-1}**	**ΔG^o kJ mol^{-1}**	**T/K**	**E_a kJ mol^{-1}**
$CoFe_2O_4$	3.533569	3.578297	-87.6462	**-0.28343**	**-8.41924**	283	**-85.2934**
	3.472222	1.909543			**-4.57227**	288	**-85.2518**
	3.412969	1.821792			**-4.43789**	293	**-85.2102**
	3.355705	1.539758			**-3.81486**	298	**-85.1687**
Composite	3.533569	0.374433	121.2015	0.428138	**-0.88099**	283	**123.55**
	3.472222	0.5463			-1.30808	288	**123.60**
	3.412969	1.363111			-3.32054	293	**123.64**
	3.355705	2.997516			-7.42656	298	123.68

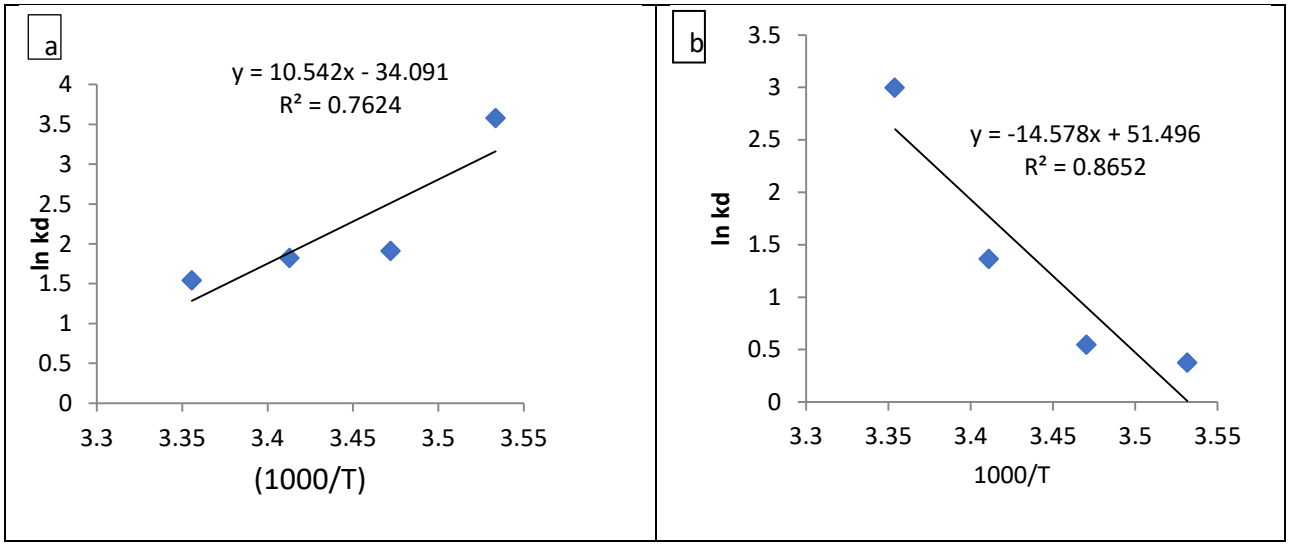

Figure (3.12): Relationship between ln kd and 1000/T for direct orange dye adsorption on a) $CoFe_2O_4$ and a) composite at **(**conditions: pH 6; dosage= 0.3 g; concentration of dye 5 mg/L**,** V=50 mL; time=45 min and temperature = (283-298 k)

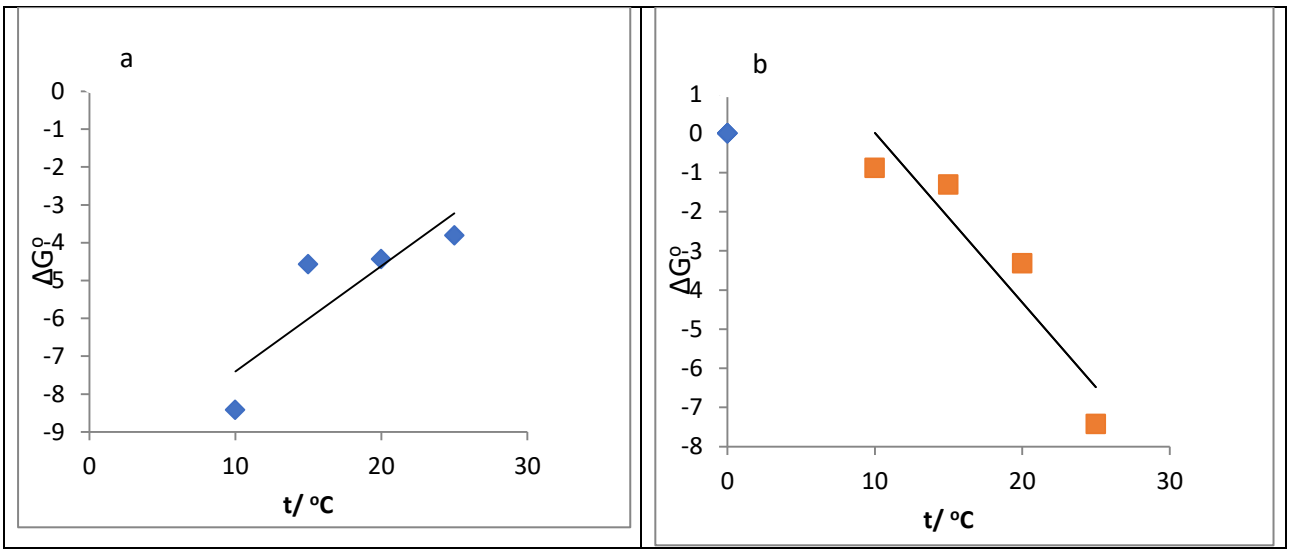

Figure (3.13): Gibb's free energy change (**ΔG^0**) against temperature for removal of dye using (a) $CoFe_2O_4$ (b) composited **(**conditions: pH 6; dosage= 0.3 g**;** concentration of dye 5 mg/L**,** V=50 mL time=45 min and temperature = (10-25) ^oC.

Table (3.8): Comparing the thermodynamics parameter results for dye adsorption on $CoFe_2O_4$ and composite.

$CoFe_2O_4$	composite
It has a negative ΔH^o (-87.6462 kJ mol^{-1}.) exothermic in nature.	It is endothermic and has a positive [94] ΔH^o 121.2015 kJ mol^{-1}).
The absolute value of ΔH^o is between 2.1 and 20.9 kJ/mol in the case of physisorption(84)	ΔH^o between 80 and 200 kJ/mol for chemisorption(84)
negative values of $\Delta S°$ indicate a decrease in the degree of freedom of the species adsorbed on the solid surface during dye adsorption(85)	value $\Delta S°$=0.428138 kJ mol Positive, this indicates an increase in randomness or entropy in the system during the process
ΔG^o values change from −8.41924 kJ mol^{-1}.to −3.81486 kJ mol^{-1}. suggests that method becomes less spontaneous (or less free energy favorable) as it progresses و the possible cause may be related to effects Surface saturation(85)	From −0.88099 to −7.42656 the ΔG^o values increase in negative magnitude, meaning that the process becomes more spontaneous with progress or change in conditions.
The E_a gradually decrease from −85.293388 kJ/mol to −85.168678 kJ/mol This slight decrease indicates that the process is becoming more thermodynamically favorable or that the system is approaching a more stable state.	E_a values gradually increase from 123.55 to 123.68 kJ/mol .This indicates that the apparent activation energy increases slightly as the process progresses.
As the temperature increased, the negative ΔG^o magnitudes reduced, indicating a favorable spontaneous reaction that does not require external energy to convert reactants into products. The magnitudes ranged from -8.41924 to -3.81486) kJ mol^{-1}, so prior studies of a similar sort are consistent with the thermodynamics findings. (86)	Values of ΔG^o-0.88099≤ ΔG ≤ -7.42656kJ/mol indicate chemisorption as the predominant mechanism involved in the dye adsorption process.

3.4. Isotherm Models for Concentration Differences in mg. L^{-1}

in the present study, the linear forms of the Langmuir and Freundlich isotherms were used not only to evaluate the adsorption capacity of dye on $CoFe_2O_4$ and composite obtained under optimum conditions but also to understand the mechanism of dye adsorption. The parameters of the dye adsorption isotherms on $CoFe_2O_4$ and composite are shown in figure 3.14 and Table 3.9.

Table (3.9). Determination coefficients, Langmuir, and Freundlich model constants for dye adsorption isotherms on $COFe_2O_4$ and its composite

Models	**Parameters**	$CoFe_2O_4$	Composite
Langmuir	R^2	0.5099	0.629
	k_L (L/mg)	0.2208	16.25696
	Q_m (mg/g)	24.3902	11.44165
Freundlich	R^2	0.4097	0.9457
	k_F (mg $g^{-1}(L.mg^{-1})^{1/n}$)	7.24	10.92.
	n	4.5788	1.402721

The coefficient of determination R^2 of the Freundlich isotherm is higher than that of the Langmuir model, as shown in table (3.9). Consequently, the Freundlich model provides a better explanation of the data obtained. This suggests that adsorption takes place on heterogeneous active sites with different binding energies. The adsorption capacity of dye is higher in composite than in cobalt ferrite. This increase in capacity may be due to reactions with organic matter adsorbed on activated carbon and poly aniline. Freundlich constant (kF) values, relative to adsorption capacity, are high, confirming the stronger adsorption of dye by composite. In addition, all n values exceed 1, indicating favorable dye adsorption(85), which ensure the adsorption types are physical and chemical using cobalt ferrite and composite, respectively. These results suggest that the Freundlich model better reflects dye removal on cobalt ferrite and composite.

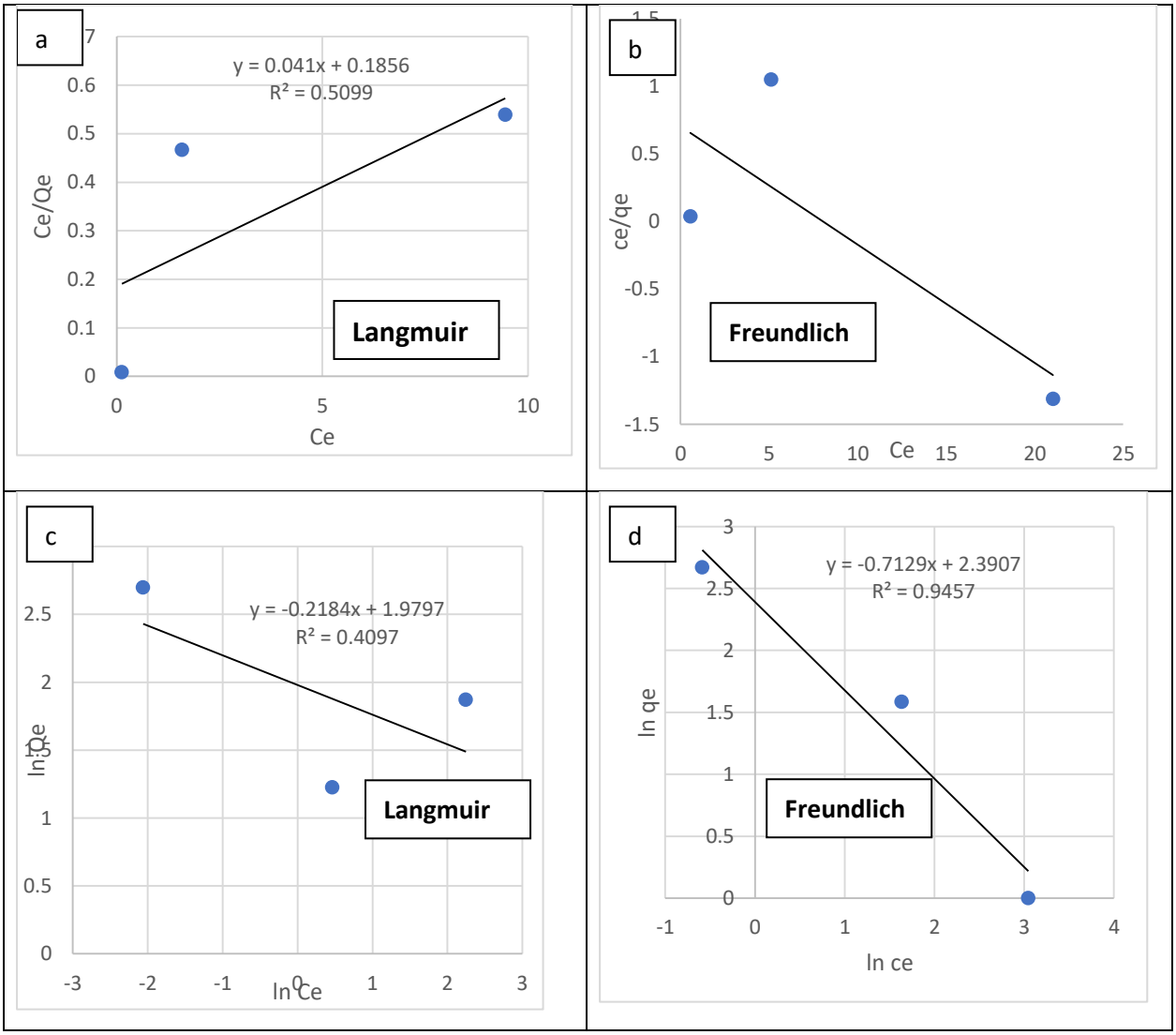

Figure (3.14). Model representations of Langmuir and Freundlich isotherms models for dye adsorption by $CoFe_2O_4$ (A and B) and composite (C and D), (conditions: pH 6; dosage= 0.3 g; different concentration of dye, V=50 mL; time=45 min and temperature = (298K)

3.5. Adsorption Kinetics

In order to identify the kinetic models, the pseudo first-order and pseudo second-order models were investigated for removal dye using $CoFe_2O_4$ and $CoFe_2O_4$\AC/PANI as shown in figures 3.16 and 3.17.

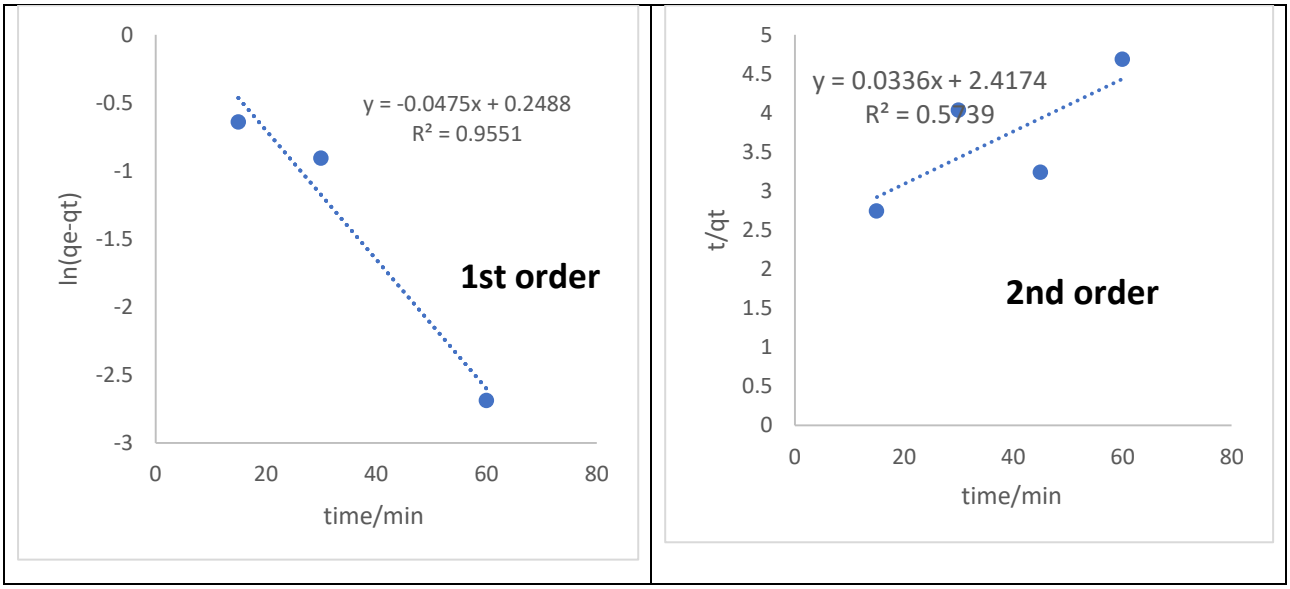

Figure (3.15): pseudo-first order kinetic model and second order for adsorption of direct orange dye on the $CoFe_2O_4$ surface **(conditions: pH 6; dosage=** 0.3 **g;** concentration of dye 5 mg/L**, V=50 mL; time=(15-60)min** and temperature = (298 k)

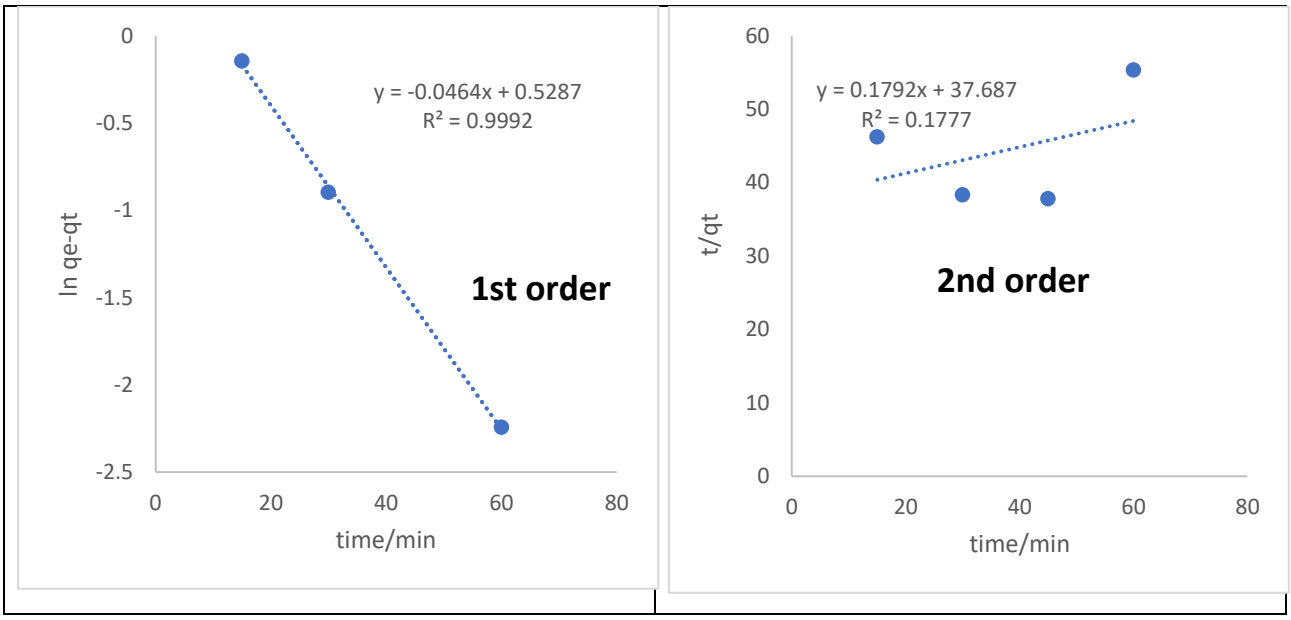

Figure (3.16) A: pseudo-first order kinetic model and second order for adsorption of direct orange dye on the composite surface. **(conditions: pH 6; dosage=** 0.3 **g;** concentration of dye 5 mg/L**, V=50 mL; time=(15-60)min** and temperature = (298 k)

The calculations for both models' kinetic constants and correlation coefficients followed equations (2.8) and (2.7) providing the findings presented in Table (3.10). The kinetic constants and correlation coefficients for both models, Based on table

3.10, The PFO model is obeyed the adsorption of direct orange 39 dye onto the $CoFe_2O_4$ /AC/ PANI and $CoFe_2O_4$ nanocomposite adsorbent, because correlation coefficient R^2 for PFO > correlation coefficient R^2 for PSO, this really case in adsorption process and agreement with the result reported in study for Kinetic study of the adsorption of dyes onto activated carbon by Eris and Bashiri(87)(88).

Table (3.10). compared between Pseudo-first order and Pseudo-first order in removal of dye using $CoFe_2O_4$ and composite

Samples	Pseudo-first order			Pseudo-second order		
	k_1	q_e	R^2	k_2	q_e	R^2
$CoFe_2O_4$	**0.0475**	1.28248551	**0.9551**	**0.007458**	1.861851	0.5739
Composite	0.0464	1.696	**0.9992**	0.000852	31.1364	0.1777

3.6. *Reusability of $CoFe_2O_4$\AC\PANI and $CoFe_2O_4$ nanoparticles.*

The data presented in Figure 3.18 and Table 3.11 highlight the reusability performance of the synthesized composite nanoparticles compared to $CoFe_2O_4$. The composite exhibited a high initial removal efficiency of 97.48%, whereas $CoFe_2O_4$ achieved 82.34%. A gradual decrease in adsorption efficiency was observed with successive reuse cycles, which can be attributed to the saturation or blockage of active sites by dye molecules and surface fouling of the nanoparticles, thus limiting adsorption capacity. Nevertheless, the composite nanoparticles maintained significant adsorption performance during the first three cycles, indicating their high potential for sustainable and cost-effective applications. Although a progressive decline was recorded after five cycles, the nanoparticles still demonstrated considerable adsorption activity with an acceptable loss in performance. These results confirm the superior reusability of the composite material compared to $CoFe_2O_4$(89) (90).

Table (3.11): Different Reusability methods achieved diverse removal percentage measurements for direct orange dye from aqueous solutions.

$(\boldsymbol{R}\ \%) = \frac{C0 - Ce}{C0} \times 100$		
step	$CoFe_2O_4$	composite
1	**82.34295**	**95.24618**
2	**44.99151**	**90.49236**
3	**32.7674**	**87.43633**
4	**28.35314**	**70.11885**
5	**23.9388**	**57.55518**

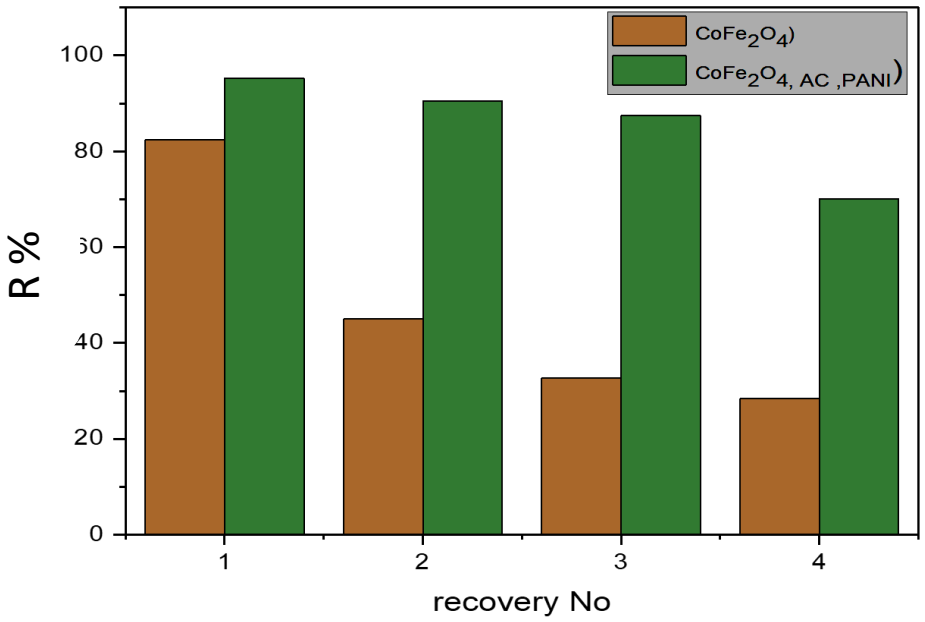

Figure 3.17. Reusability of $CoFe_2O_4$NPs and composite surface for direct orange dye adsorption. **(**conditions: pH 6**;** dosage**=** 0.3 g**; 5** mg. L^{-1} of dye, V=50 mL; time=45 min; T=298 K)

3.7. Conclusions

1. $CoFe_2O_4$ and AC/PANI Nanoparticle were successfully Synthesized.

2. FT-IR, XRD, BET and SEM techniques were used to analyze and confirm the synthesized $CoFe_2O_4$, and composite nanoparticles.

3. The mean crystal sizes of $CoFe_2O_4$ elevates from 31.83 nm to 36 nm after change to composite.

4. The maximum removal of 5 $mg.\ L^{-1}$ direct orange 39dye from an aqueous solution using $CoFe_2O_4$, and its composite was found at 45 minutes and pH 6, 0.3g of adsorbents.

5. Thermodynamic studies revealed that sorption of dye on to $CoFe_2O_4$, and composite was done, and the enthalpies (ΔH) were -87.6462 kJ/mol (exothermic) and 121.2015kJ/mol (endothermic) respectively.

6. Kinetic studies have indicated that the reaction using composite is obeyed pseudo- first order.

7. The Freundlich model is more applied than Langmuir model and proved the types of adsorptions are physical and chemical using $CoFe_2O_4$, and composite respectively.

8. The reuse of $CoFe_2O_4$ and composite surfaces via removal of dye demonstrates the composite surface is more active than $CoFe_2O_4$ surface.

3.8. Future Studies

1. The $CoFe_2O_4$ and composite nanoparticles can be resynthesized by green route to be as environmentally-friendly method with different shapes and sizes.
2. Surface characterization methods such as TGA, XPS and Raman spectroscopy can be estimated to detect the additive properties that enhanced the synthesis process.

3. Investigating the impact of other parameters on the adsorption process, including ionic intensity, surfactant content, and shaking speed.
4. Tests evaluate the biological properties of final products.
5. Test the mechanical properties together with electrical properties of manufactured materials.

References

1. Karaj I. Raw and modified rice husk performance in removal of Basic Blue 41 from aqueous solutions. J Occup Environ Heal. 2016;1(1):41–9.

2. Chikwe TN, Ekpo RE, Okoye I. Competitive adsorption of organic solvents using modified and unmodified calcium bentonite clay mineral. Chem Int. 2018;4(4):230–9.

3. Dey PC, Das R. Effect of silver doping on the elastic properties of CdS nanoparticles. Indian J Phys. 2018;92:1099–108.

4. Meva FE, Ntoumba AA, Kedi PBE, Tchoumbi E, Schmitz A, Schmolke L, et al. Silver and palladium nanoparticles produced using a plant extract as reducing agent, stabilized with an ionic liquid: sizing by X-ray powder diffraction and dynamic light scattering. J Mater Res Technol. 2019;8(2):1991–2000.

5. Farrokhi M, Hosseini SC, Yang JK, Shirzad-Siboni M. Application of ZnO–Fe 3 O 4 nanocomposite on the removal of azo dye from aqueous solutions: kinetics and equilibrium studies. Water, Air, Soil Pollut. 2014;225:1–12.

6. Zare EN, Motahari A, Sillanpää M. Nanoadsorbents based on conducting polymer nanocomposites with main focus on polyaniline and its derivatives for removal of heavy metal ions/dyes: a review. Environ Res. 2018;162:173–95.

7. Janaki V, Kamala-Kannan S, Shanthi K. Significance of Indian peat moss for the removal of Ni (II) ions from aqueous solution. Environ Earth Sci. 2015;74:5351–7.

8. Shahabuddin M, Bhattacharya S. Enhancement of performance and emission characteristics by co-gasification of biomass and coal using an entrained flow gasifier. J Energy Inst. 2021;95:166–78.

9. Mishra RK, Mentha SS, Misra Y, Dwivedi N. Emerging pollutants of severe environmental concern in water and wastewater: A comprehensive review on current developments and future research. Water-Energy Nexus. 2023;

10. Punzi M, Nilsson F, Anbalagan A, Svensson BM, Jönsson K, Mattiasson B, et al. Combined anaerobic–ozonation process for treatment of textile wastewater: removal of acute toxicity and mutagenicity. J Hazard Mater. 2015;292:52–60.

11. Cooksey CJ. Quirks of dye nomenclature. 10. Eosin Y and its close relatives. Biotech Histochem. 2018;93(3):211–9.

12. Clark M. Handbook of textile and industrial dyeing: principles, processes and types of dyes. Elsevier; 2011.

13. Zollinger H. Color chemistry: syntheses, properties, and applications of organic dyes and pigments. John Wiley & Sons; 2003.

14. Fard ZM, Bagheri M, Rabieh S, Mousavi HZ. Synthesis of hierarchical RGO@ Cu2O@ Cu nanocomposites: optimization of photocatalytic degradation of Direct Orange 39 using a response surface methodology. J Mater Sci Mater Electron. 2017;28(13):9618.

15. Mathew DS, Juang RS. An overview of the structure and magnetism of spinel ferrite nanoparticles and their synthesis in microemulsions. Chem Eng J. 2007;129(1–3):51–65.

16. Burkinshaw SM. Physico-chemical aspects of textile coloration. John Wiley & Sons; 2016.

17. Abbas M. Valorisation du noyau d'abricot dans la depollution des eaux. 2015.

18. Ravi VP, Jasra R V, Bhat TSG. Adsorption of phenol, cresol isomers and benzyl alcohol from aqueous solution on activated carbon at 278, 298 and 323 K. J Chem Technol Biotechnol Int Res Process Environ Clean Technol. 1998;71(2):173–9.

19. Puccia V, Avena MJ. On the use of the Dubinin-Radushkevich equation to distinguish between physical and chemical adsorption at the solid-water interface. Colloid Interface Sci Commun. 2021;41:100376.

20. Xia M, Chen Z, Li Y, Li C, Ahmad NM, Cheema WA, et al. Removal of Hg (II) in aqueous solutions through physical and chemical adsorption principles. RSC Adv. 2019;9(36):20941–53.

21. Gerasimov AI. Water as an insulator in pulsed facilities. Instruments Exp Tech. 2005;48:141–67.

22. Tawfeeq IM, Mohammed AJ. Adsorption Ability and Kinetic of (Congo Red, Methyl Green) Dyes on Iraqi Siliceous Rocks. J Glob Pharma Technol. 2009;11(07).

23. Iryani A, Nur H, Santoso M, Hartanto D. Adsorption study of rhodamine B and methylene blue dyes with ZSM-5 directly synthesized from Bangka Kaolin without organic template. Indones

J Chem. 2020;20(1):130–40.

24. Jiuhui QU. Research progress of novel adsorption processes in water purification: a review. J Environ Sci. 2008;20(1):1–13.

25. Barry D, Cook M. Adsorption of cyclohexane and benzene on two modified silica supports. J Phys Chem. 1975;79(23):2555–62.

26. Dąbrowski A. Adsorption—from theory to practice. Adv Colloid Interface Sci. 2001;93(1–3):135–224.

27. CH G. Studies in adsorption. Part XI. A system of classification of solution adsorption isotherms, and its use in diagnosis of adsorption mechanisms and in measurements of specific surface areas of solids. J Chem Soc. 1960;786:3973–93.

28. Guler UA, Ersan M, Tuncel E, Dügenci F. Mono and simultaneous removal of crystal violet and safranin dyes from aqueous solutions by HDTMA-modified Spirulina sp. Process Saf Environ Prot. 2016;99:194–206.

29. Bozorgian A. Investigation and comparison of experimental data of ethylene dichloride adsorption by Bagasse with adsorption isotherm models. Chem Rev Lett. 2020;3(2):79–85.

30. Edet UA, Ifelebuegu AO. Kinetics, isotherms, and thermodynamic modeling of the adsorption of phosphates from model wastewater using recycled brick waste. Processes. 2020;8(6):665.

31. Cardenas C, Farrusseng D, Daniel C, Aubry R. Modeling of equilibrium water vapor adsorption isotherms on activated carbon, alumina and hopcalite. Fluid Phase Equilib. 2022;561:113520.

32. Das A, Chatterjee S, Suresh Kumar G. Targeting human telomeric G-quadruplex DNA with antitumour natural alkaloid aristololactam-β-D-glucoside and its comparison with daunomycin. J Mol Recognit. 2017;30(10):e2639.

33. Gouamid M, Ouahrani MR, Bensaci MB. Adsorption equilibrium, kinetics and thermodynamics of methylene blue from aqueous solutions using date palm leaves. Energy procedia. 2013;36:898–907.

34. AlOthman ZA, Habila MA, Ali R, Ghafar AA, Hassouna MSE din. Valorization of two waste streams into activated carbon and studying its adsorption kinetics, equilibrium isotherms and thermodynamics for methylene blue removal. Arab J Chem.

2014;7(6):1148–58.

35. Williams CK. Thermodynamic parameters obtained from the van’t hoff analysis of the binding of bile salts by cationic adsorbents. 2002;

36. Taylor HS. The activation energy of adsorption processes. J Am Chem Soc. 1931;53(2):578–97.

37. Ghosh S, Ray A, Pramanik N. Self-assembly of surfactants: An overview on general aspects of amphiphiles. Biophys Chem. 2020;265:106429.

38. de Guertechin LO. Surfactants: classification. In: Handbook of detergents, part A. CRC Press; 1999. p. 7–46.

39. Xu X, Gao Z, Cui Z, Liang Y, Li Z, Zhu S, et al. Synthesis of Cu2O octadecahedron/TiO2 quantum dot heterojunctions with high visible light photocatalytic activity and high stability. ACS Appl Mater Interfaces. 2016;8(1):91–101.

40. Zinovjev K, Tuñón I. Reaction coordinates and transition states in enzymatic catalysis. Wiley Interdiscip Rev Comput Mol Sci. 2018;8(1):e1329.

41. Cheng M, Zeng G, Huang D, Yang C, Lai C, Zhang C, et al. Tween 80 surfactant-enhanced bioremediation: toward a solution to the soil contamination by hydrophobic organic compounds. Crit Rev Biotechnol. 2018;38(1):17–30.

42. Rosen MJ, Kunjappu JT. Surfactants and interfacial phenomena. John Wiley & Sons; 2012.

43. El-Okr MM, Salem MA, Salim MS, El-Okr RM, Ashoush M, Talaat HM. Synthesis of cobalt ferrite nano-particles and their magnetic characterization. J Magn Magn Mater. 2011;323(7):920–6.

44. Houshiar M, Zebhi F, Razi ZJ, Alidoust A, Askari Z. Synthesis of cobalt ferrite (CoFe2O4) nanoparticles using combustion, coprecipitation, and precipitation methods: A comparison study of size, structural, and magnetic properties. J Magn Magn Mater. 2014;371:43–8.

45. Ristic M, Krehula S, Reissner M, Jean M, Hannoyer B, Musić S. Synthesis and properties of precipitated cobalt ferrite nanoparticles. J Mol Struct. 2017;1140:32–8.

46. Refat NM, Nassar MY, Sadeek SA. A controllable one-pot hydrothermal synthesis of spherical cobalt ferrite nanoparticles: synthesis, characterization, and optical properties. RSC Adv. 2022;12(38):25081–95.

47. Gomes P, Costa B, Carvalho JPF, Soares PIP, Vieira T, Henriques C, et al. Cobalt Ferrite Synthesized Using a Biogenic Sol–Gel Method for Biomedical Applications. Molecules. 2023;28(23):7737.

48. Leng C, Wei J, Liu Z, Xiong R, Pan C, Shi J. Facile synthesis of PANI-modified CoFe 2 O 4–TiO 2 hierarchical flower-like nanoarchitectures with high photocatalytic activity. J nanoparticle Res. 2013;15:1–11.

49. Mohanraju K, Sreejith V, Ananth R, Cindrella L. Enhanced electrocatalytic activity of PANI and CoFe2O4/PANI composite supported on graphene for fuel cell applications. J Power Sources. 2015;284:383–91.

50. Sankar KV, Selvan RK. Fabrication of flexible fiber supercapacitor using covalently grafted CoFe2O4/reduced graphene oxide/polyaniline and its electrochemical performances. Electrochim Acta. 2016;213:469–81.

51. Barik B, Sahoo SJ, Maji B, Bag J, Mishra M, Dash P. Microwave-Assisted Development of Magnetically Recyclable PANI-Modified CoFe2O4-WO3 p–n–n Heterojunction: A Visible-Light-Driven Photocatalyst for Antibiotic Toxicity Reduction. Ind Eng Chem Res. 2021;60(42):15125–40.

52. Singh S, Kaur P, Aggarwal D, Kumar V, Tikoo K, Bansal S, et al. Polyaniline enwrapped CoFe2O4/g-CN ternary nanocomposite for adsorption driven photocatalytic degradation of explicitly diverse organic pollutants. J Alloys Compd. 2022;923:166255.

53. Gabal MA, Al-Mutairi E, Al Angari YM, Salam MA, Awad A, Al-Juaid AA, et al. CoFe2O4/PANI/MWCNTs ternary hybrid composites. Synthesis, characterization, the effect of MWCNTs ratio and dye removal capability. Environ Sci Pollut Res. 2024;1–14.

54. Hasan Taresh B, Hadi Fakhri F, M Ahmed L. Synthesis and characterization of CuO/CeO2 nanocomposites and investigation their photocatalytic activity. J Nanostructures. 2022;12(3):563–70.

55. Havrdova M, Polakova K, Skopalik J, Vujtek M, Mokdad A, Homolkova M, et al. Field emission scanning electron microscopy (FE-SEM) as an approach for nanoparticle detection inside cells. Micron. 2014;67:149–54.

56. Jawad TM, Ahmed LM. DIRECT ULTRASONIC SYNTHESIS OF WO 3/TiO 2 NANOCOMPOSITES AND APPLYING THEM IN THE PHOTODECOLORIZATION OF EOSIN YELLOW DYE. Periódico Tchê Química. 2020;17(34).

57. Mohammad AM, Ridha SMA, Mubarak TH. Dielectric properties of Cr-substituted cobalt ferrite nanoparticles synthesis by citrate-gel auto combustion method. Int J Appl Eng Res. 2018;13(8):6026–35.

58. Goodarz Naseri M, Saion EB, Abbastabar Ahangar H, Shaari AH, Hashim M. Simple synthesis and characterization of cobalt ferrite nanoparticles by a thermal treatment method. J Nanomater. 2010;2010(1):907686.

59. Li J, Xiao Q, Li L, Shen J, Hu D. Novel ternary composites: Preparation, performance and application of ZnFe 2 O 4 /TiO 2 /polyaniline. Appl Surf Sci [Internet]. 2015;331:108–14. Available from: http://dx.doi.org/10.1016/j.apsusc.2015.01.001

60. Galal A, Sadek O, Soliman M, Ebrahim S, Anas M. Synthesis of nanosized nickel zinc ferrite using electric arc furnace dust and ferrous pickle liquor. Sci Rep. 2021;11(1):1–11.

61. Auta M, Hameed BH. Optimized waste tea activated carbon for adsorption of Methylene Blue and Acid Blue 29 dyes using response surface methodology. Chem Eng J. 2011;175:233–43.

62. Rakshit R, Khatun E, Pal M, Talukdar S, Mandal D, Saha P, et al. Influence of functional group of dye on the adsorption behaviour of CoFe 2 O 4 nano-hollow spheres. New J Chem. 2017;41(17):9095–102.

63. Swenson H, Stadie NP. Langmuir's theory of adsorption: A centennial review. Langmuir. 2019;35(16):5409–26.

64. Law WM, Lau WN, Lo KL, Wai LM, Chiu SW. Removal of biocide pentachlorophenol in water system by the spent mushroom compost of Pleurotus pulmonarius. Chemosphere. 2003;52(9):1531–7.

65. Ai L, Huang H, Chen Z, Wei X, Jiang J. Activated carbon/CoFe2O4 composites: facile synthesis, magnetic

performance and their potential application for the removal of malachite green from water. Chem Eng J. 2010;156(2):243–9.

66. Ho YS, McKay G. Sorption of dye from aqueous solution by peat. Chem Eng J. 1998;70(2):115–24.

67. Tarq N, Sadoon H, Alshammari A. Characterization of cobalt ferrite nanoparticle and evaluation its toxic effect in experimental mice: Characterization of cobalt ferrite nanoparticle and evaluation its toxic effect in experimental mice. Acta Vet Bras. 2024;18(2).

68. Ibeniaich M, Elansary M, Minaoui K, Mouhib Y, El Haj YA, Belaiche Y, et al. Exploring the effect of Hf (IV) doping in spinel ferrite CoHfxFe2-xO4 on magnetic properties, electrochemical impedance, and photocatalytic activity: In-depth structural study. J Mol Struct. 2024;1318:139395.

69. Tian Y, Fan X, Chen K, Chen X, Peng W, Wang L, et al. Optical biomarker analysis for renal cell carcinoma obtained from preoperative and postoperative patients using ATR-FTIR spectroscopy. Spectrochim Acta Part A Mol Biomol Spectrosc. 2024;318:124426.

70. Durig DT. Conformational analysis of some halo or pseudohalo substituted small organic molecules by spectroscopic and theoretical methods. University of South Carolina; 1987.

71. Abd Ali LI, Ismail HK, Alesary HF, Aboul-Enein HY. Correction to: A nanocomposite based on polyaniline, nickel and manganese oxides for dye removal from aqueous solutions. Int J Environ Sci Technol. 2021;18(7):2051.

72. Li XH, Xu CL, Han XH, Qiao L, Wang T, Li FS. Synthesis and magnetic properties of nearly monodisperse CoFe 2 O 4 nanoparticles through a simple hydrothermal condition. Nanoscale Res Lett. 2010;5:1039–44.

73. Kalam A, Al-Sehemi AG, Assiri M, Du G, Ahmad T, Ahmad I, et al. Modified solvothermal synthesis of cobalt ferrite (CoFe2O4) magnetic nanoparticles photocatalysts for degradation of methylene blue with H2O2/visible light. Results Phys. 2018;8:1046–53.

74. Mohammadi Z, Attaran N, Sazgarnia A, Shaegh SAM, Montazerabadi A. Superparamagnetic cobalt ferrite nanoparticles as T 2 contrast agent in MRI: in vitro study. IET nanobiotechnology. 2020;14(5):396–404.

75. Malinowska I, Ryżyńska Z, Mrotek E, Klimczuk T, Zielińska-Jurek A. Synthesis of CoFe2O4 nanoparticles: the effect of ionic strength, concentration, and precursor type on morphology and magnetic properties. J Nanomater. 2020;2020(1):9046219.

76. El-Kady AA, Abdel Ghafar HH, Ibrahim MBM, Abdel-Wahhab MA. Utilization of activated carbon prepared from agricultural waste for the removal of organophosphorous pesticide from aqueous media. Desalin Water Treat. 2013;51(37–39):7276–85.

77. Donohue MD, Aranovich GL. Classification of Gibbs adsorption isotherms. Adv Colloid Interface Sci. 1998;76:137–52.

78. Ambroz F, Macdonald TJ, Martis V, Parkin IP. Evaluation of the BET Theory for the Characterization of Meso and Microporous MOFs. Small methods. 2018;2(11):1800173.

79. DEBOER JH. The dynamical character of adsorption. Vol. 76. LWW; 1953.

80. Liu XM, Fu SY, Huang CJ. Synthesis and magnetic characterization of novel CoFe2O4–BiFeO3 nanocomposites. Mater Sci Eng B. 2005;121(3):255–60.

81. Varghese D, S. R N, P JSJ. Synergistic design of $CuO/CoFe_2O_4$/MWCNTs ternary nanocomposite for enhanced photocatalytic degradation of tetracycline under visible light. Sci Rep. 2025;15(1):320.

82. Baseri JR, Palanisamy PN, Sivakumar P. Comparative studies of the adsorption of direct dye on activated carbon and conducting polymer composite. J Chem. 2012;9(3):1122–34.

83. Kumar S, Goel E, Singh K, Singh B, Kumar M, Jit S. A compact 2-D analytical model for electrical characteristics of double-gate tunnel field-effect transistors with a SiO 2/High-$ k $ stacked gate-oxide structure. IEEE Trans Electron Devices. 2016;63(8):3291–9.

84. Kiari MNA, Konan ATS, Mamane OS, Ouattara LY, Grema MHI, Boukari MSD, et al. Adsorption kinetics, thermodynamics, modeling and optimization of bisphenol A on activated carbon based on Hyphaene Thebaica shells. Case Stud Chem Environ Eng. 2024;10:100903.

85. Garikoé I, Sorgho B, Yaméogo A, Guel B, Andala D. Removal of bisphenol A by adsorption on organically modified clays from Burkina Faso. Bioremediat J. 2020;25(1):22–47.

86. Greaves RJ, Schlecht KD. Gibbs free energy: The criteria for spontaneity. J Chem Educ. 1992;69(5):417.

87. Eris S, Bashiri H. Kinetic study of the adsorption of dyes onto activated carbon. Prog React Kinet Mech. 2016;41(2):109–19.

88. Simonescu CM, Tătăruş A, Culiţă DC, Stănică N, Butoi B, Kuncser A. Facile synthesis of cobalt ferrite (CoFe2O4) nanoparticles in the presence of sodium bis (2-ethyl-hexyl) sulfosuccinate and their application in dyes removal from single and binary aqueous solutions. Nanomaterials. 2021;11(11):3128.

89. Borgohain X, Das E, Rashid MH. Facile synthesis of CeO 2 nanoparticles for enhanced removal of malachite green dye from an aqueous environment. Mater Adv. 2023;4(2):683–93.

90. Thamer BM, Al-aizari FA. Highly efficient and reusable polymeric nanofibers for cationic dye removal: isotherm, kinetics and thermodynamic study. New J Chem. 2024;48(3):1414–23.

الخلاصة

يتضمن هذا العمل ثلاثة أجزاء، يستخدم الجزء الأول منها عملية ترسيب جديدة لتخليق جسيمات الكوبالت الفراتية ($CoFe_2O_4$) النانوية باستخدام السيترامايد (CT) كمادة خافضة للتوتر السطحي إيجابية. تم تخليق جسيمات $CoFe_2O_4$ النانوية على هيئة سبينل معكوس. تم إنشاء المركب النانوي PANI/$CoFe_2O_4$/Ac باستخدام عملية بلمرة الأكسدة الكيميائية باستخدام حمض الهيدروكلوريك والأمونيوم بير سلفات (APS) كمنشطات ومؤكسدات.

من خلال الجزء الثاني، تم تحديد جسيمات $CoFe_2O_4$ النانوية الإسبنيل $CoFe_2O_4$ ومركباتها باستخدام عدة تقنيات. وأظهر التحليل الطيفي بالأشعة تحت الحمراء قممًا مميزة بين 600 و400 سم-1، مما يشير إلى مواقع الأشكال الرباعية السطوح Fe-O والثمانية السطوح Co-O في جسيمات $CoFe_2O_4$ النانوية. وأظهر حيود الأشعة السينية أن العينات المحضرة من $CoFe_2O_4$ ومركبها الثلاثي لها حجم نانوي يتراوح من 31.83 نانومتر لـ $CoFe_2O_4$ إلى 36 نانومتر للمركب الثلاثي. أظهرت صورة SEM فكرة عن التشكل السطحي للمركبات المحضرة، وقد وُجد أن شكل الإسبنيل $CoFe_2O_4$ يشبه النسيج، ولكن بالنسبة للمركب وجد أنه ذو طبقات، كما وُجد أن أحجام الجسيمات المقاسة للإسبنيل تتراوح بين 33.03 إلى 41.35 نانومتر، وبالنسبة للمركب يساوي 29.34 إلى 49.90 نانومتر، وبالتالي فإن جميع العينات التي تمت دراستها تعتبر بلورات نانوية. أظهرت أطياف EDX أن عناصر Co وFe وO وC في المحفز كانت موجودة ونقية بدون شوائب. تم قياس مساحات سطح BET وتوزيع حجم المسام لكل من العينات التركيبية وأثبتت أن حلقات التباطؤ تتوافق مع متساوي الامتزاز من النوع الرابع، وحلقة التباطؤ في نطاق الضغط النسبي (P/P0) من 0.3 ~ 1.0، والتي تنتمي إلى النوع H3 مع المسام النانوية. وتزيد مساحة السطح المحددة للمركب الثلاثي عن قيمة فريت الكوبالت وتساوي 54.118 م2 جم-1 و8.9064 م2 جم-1 على التوالي

في الجزء الثالث، تم استخدام جسيمات الكوبالت الفيريت النانوية ومركبها كمادة ماصة لإزالة الصبغة البرتقالية المباشرة من المحاليل المائية. في البداية، تم إجراء تجربة الامتزاز لجميع الأسطح المحضرة تجاه الصبغة وتم العثور على أعلى نسبة لإزالة الصبغة على السطح المتراكب حيث بلغ معدل الإزالة 95%.

تم العثور على كفاءة إزالة الصبغة البرتقالية المباشرة عند 45 دقيقة كوقت توازن أمثل، وكتلة السطح عند 0.3 جم، ودرجة الحموضة 6. بعد ذلك، تمت دراسة العوامل المؤثرة على عملية الامتزاز (الوقت، التركيز، الوزن، درجة الحموضة، درجة الحرارة) لسطح فريت الكوبالت والمركب الثلاثي، وأعطى المركب الثلاثي كفاءة إزالة أعلى مقارنة بفريت الكوبالت. في قابلية إعادة الاستخدام، وجد أنه بعد أربع دورات، انخفضت كفاءة إزالة الصبغة للمركب من 95.24% إلى 70.11%، بينما انخفضت كفاءة إزالة الصبغة لفريت الكوبالت من 82.34% إلى 28.35%. تشير هذه النتائج إلى أن المركب يظهر قابلية أعلى لإعادة الاستخدام مقارنة بفريت الكوبالت. ومن ناحية أخرى، تم الكشف عن دوال الديناميكا الحرارية ووجد أن تفاعل إزالة الصبغة بواسطة $CoFe_2O_4$ طارد للحرارة مع امتزاز فيزيائي (أقل من 40 كيلوجول/مول)، وهو ما يتفق مع النتيجة من خلال معادلة فروندليتش التطبيقية، في حين أن نفس التفاعل باستخدام المركب أظهر امتزازًا كيميائيًا (أكبر من 80 كيلوجول/مول) مع تفاعل ماص للحرارة يتم اتباع نموذج PFO لامتصاص الصبغة البرتقالية المباشرة 39 على المادة الماصة النانوية PANI /AC/ $CoFe_2O_4$ و$CoFe_2O_4$، لأن معامل الارتباط R^2 لـ PFO > معامل الارتباط R^2 لـ PSO،

جامعه كربلاء

كليه العلوم

قسم الكيمياء

تحضير وتوصيف $CoFe_2O_4$ / active carbon/ / polyaniline كمتراكب ثلاثي وتطبيقاته في معالجة الماء

رسالة مقدمه الى مجلس كليه العلوم جامعه كربلاء وهي جزء من متطلبات نيل درجه الماجستير في علوم الكيمياء

من قبل

محمد فاضل هاتف

بإشراف

ا. د. لمى مجيد احمد

ا. م. د. حسن فيصل نعمه

2025 م

1446ه